AECL-10782

ATOMIC ENERGY OF CANADA LIMITED

ÉNERGIE ATOMIQUE DU CANADA LIMITÉE

MECHANICAL DESIGN DEVELOPMENT OF A 476 MHz RF CAVITY FOR THE PEP-II ASYMMETRIC B-FACTORY

MISE AU POINT DE LA CONCEPTION MÉCANIQUE D'UNE CAVITÉ À CHAMP DE R-F DE 476 MHz DE L'ACCÉLÉRATEUR DU PROJET PEP-II B FACTORY

M.S. de JONG, T. TRAN-NGOC, F.P. ADAMS, M.G. LIPSETT and W. MELLORS

Chalk River Laboratories

Laboratoires de Chalk River

Chalk River, Ontario K0J 1J0

February 1993 février

AECL Research

MECHANICAL DESIGN DEVELOPMENT OF A 476 MHz RF CAVITY FOR THE PEP-II ASYMMETRIC B-FACTORY

by

M.S. de Jong, T. Tran-Ngoc, F.P. Adams,
M.G. Lipsett and W. Mellors

Accelerator Physics Branch
Chalk River Laboratories
Chalk River, Ontario, K0J 1J0
1993 February

AECL-10782

EACL Recherche

MISE AU POINT DE LA CONCEPTION MÉCANIQUE D'UNE CAVITÉ À CHAMP DE R-F DE 476 MHz DE L'ACCÉLÉRATEUR DU PROJET PEP-II B-FACTORY

par

M.S. de Jong, T. Tran-Ngoc, F.P. Adams,
M.G. Lipsett et W. Mellors

RÉSUMÉ

Dans le présent rapport, on décrit la mise au point d'une conception mécanique d'une cavité à une sele cellule à champ de R-F de 476 MHz convenant à l'accélérateur du Projet PEP-II B-Factory du Stanford Linear Accelerator Center (Centre d'accélérateurs linéaires de Stanford). Les travaux ont compris la conception mécanique préliminaire d'une cavité à une seule cellule à champ de R-F de 476 MHz pouvant résister à une dissipation de 150 kW dans les parois de la cavité. On y présente les résultats d'analyses poussées bidimensionnelles et tridimensionnelles du transfert de chaleur et des contraintes thermiques de la structure de la cavité dans des conditions de fonctionnement à haute puissance et on propose un plan de conception mécanique et fabrication.

Ces travaux sont soutenus par le U.S. Department of Energy (Ministère de l'énergie des É.-U.) sous le contrat DE-AC03-76SF00515.

Physique des accélérateurs
Laboratories de Chalk River
Chalk River (Ontario) K0J 1J0
1993 février

AECL-10782

AECL Research

MECHANICAL DESIGN DEVELOPMENT OF A 476 MHz RF CAVITY FOR THE PEP-II ASYMMETRIC B-FACTORY

by

M.S. de Jong, T. Tran-Ngoc, F.P. Adams,
M.G. Lipsett and W. Mellors

ABSTRACT

This report describes the development of a mechanical design for a single-cell 476 MHz room-temperature rf cavity suitable for the PEP-II Asymmetric B-Factory Project at the Stanford Linear Accelerator Center. The work comprised preparation of a preliminary mechanical design of a single-cell 476 MHz rf cavity capable of handling 150 kW dissipation in the cavity walls. The results of extensive 2-dimensional and 3-dimensional heat-transfer and thermal-stress analyses of the cavity structure under high-power operating conditions are presented, and a mechanical design and fabrication scheme is proposed.

This work is supported by U.S. Department of Energy, contract DE-AC03-76SF00515.

Accelerator Physics Branch
Chalk River Laboratories
Chalk River, Ontario, K0J 1J0
1993 February

AECL-10782

CONTENTS

LIST OF TABLES

LIST OF FIGURES

Page

Page

Page

1. INTRODUCTION

This report describes work performed by AECL Research, Chalk River Laboratories, as part of a collaboration between Chalk River Laboratories and the Stanford Linear Accelerator Center (SLAC), the Lawrence Berkeley Laboratory (LBL), and the Lawrence Livermore National Laboratory (LLNL) to develop a prototype high-power 476 MHz rf cavity suitable for the PEP-II Asymmetric B-Factory at SLAC. The work comprises:

- a preliminary analysis, where the basic information that constrains the mechanical design, such as total dissipated power and maximum water temperature rise, is reviewed and some immediate consequences are deduced;
- a 2-dimensional (2-D) heat-transfer and thermal-stress analysis, where initial cooling and mechanical designs are evaluated;
- a 3-dimensional (3-D) heat-transfer and thermal-stress analysis that emphasizes those specific design aspects that cannot be examined with the 2-D analysis; and
- a cavity fabrication analysis, where an approach to manufacturing the cavity is developed, consistent with the results of the heat-transfer and thermal-stress analyses and with the general design constraints.

2. PRELIMINARY DESIGN CONSIDERATIONS

Several general considerations are essential background for the development of a cavity design. These include the rf properties of the cavity that affect the mechanical design and the engineering mechanical design guidelines for accelerator cavities.

The basic rf design problem for a normal-conducting cavity is to maximize the fundamental mode shunt impedance while minimizing the higher-order-mode (HOM) shunt impedances--in effect, maximize the fundamental mode cavity voltage, as seen by the beam, for a given input power at the drive rf frequency, while minimizing the voltage induced by the beam at the other frequencies. This rf design is the first and foremost step in cavity design: the main effects of the rf system on the beam are determined in this step.

Typically, this procedure involves computation of these impedances for many variations of the cavity geometry using 2-D rf codes, such as SUPERFISH [1], and 3-D rf codes, such as MAFIA [2] and ARGUS [3]. Such computations for the PEP-II cavity [4] have resulted in a design with parameters given in Table 1, where the cavity wall material is assumed to be oxygen-free high-conductivity (OFHC) copper.

In addition to the rf design, several important thermal and mechanical specifications constrain the development of cavity mechanical design. These relate to the properties of the coolants used, allowable materials and engineering design guidelines for specific applications. While these specifications are often not binding, they represent accepted practice in the field and should not be exceeded without substantial justification and analysis of alternative

Table 1: PEP-II Cavity RF Parameters

RF Frequency [MHz]	476
Shunt Impedance [MΩ]	3.5
Wall Losses (max.) [kW]	150
Voltage (min.) [MV]	0.93
Power to Beam (max.) [kW]	360

Table 2: Cavity Cooling Specifications

Input cooling water temperature	35°C
Maximum cavity-vacuum surface temperature	150°C
Maximum cavity-water surface temperature	100°C
Maximum bulk water temperature change	10°C
Maximum cooling water pressure	1.7 MPa
Hydrostatic test pressure (twice operating pressure)	3.4 MPa

approaches. Table 2 gives the maximum design operating conditions for the water cooling system used on PEP-II.

3. 2-D ANALYSIS

A 2-D heat-transfer and thermal-stress analysis is used initially, to determine the basic layout of cooling channels and survey alternative designs for possible compromises between cavity deformation and maximum stress. Once the basic design is settled, a more detailed and time-consuming 3-D heat-transfer and thermal-stress analysis is performed. All heat-transfer and thermal-stress analyses are made with the MARC and MENTAT [5] finite-element computer codes. A finite-element model of the PEP-II cavity used for initial 2-D heat-transfer and thermal-stress analysis is shown in Figure 1. In this model, the HOM waveguide ports must be omitted, as well as other apertures in the cavity walls for the tuner and rf drive line, as these features are axially asymmetric.

A total of 230 axially symmetric, four-node, isoparametric quadrilateral finite elements and 282 nodes are used to model the cavity, which has a 22 mm wall thickness. The inner shell between the interior and the cooling channels is 6 mm thick and the cooling channels are 10 mm square. Cavity mid-plane symmetry permits simulation of only one half of the cavity. Zero heat flux and zero axial displacement are imposed as boundary conditions on the plane of symmetry in the heat-transfer and thermal-stress analysis, respectively. The model includes a fine mesh between one cooling channel and the inside surface of the cavity, to allow a detailed analysis of the local deformation of the cavity wall due to water pressure.

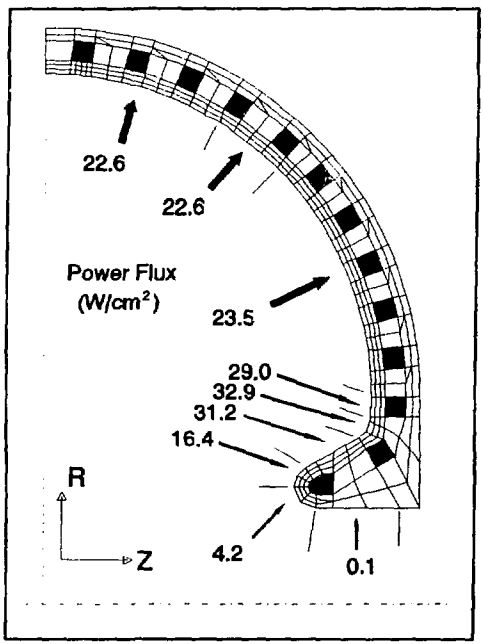

Figure 1: Two-dimensional finite-element model for PEP-II heat transfer and stress analyses

The result required from the rf codes for the heat transfer analysis is the power flux distribution, F, of rf dissipation over the internal surfaces and the cavity geometry. The tangential surface magnetic fields, $\mathbf{H}_{tan}$, determine F by:

$$F = \tfrac{1}{2}[(\omega \mu / 2\sigma)^{1/2} |\mathbf{H}_{tan}|^2] \qquad (1)$$

where ω, μ and σ are the angular frequency, cavity wall rf permeability and conductivity,

respectively. The power flux distribution used in the 2-D PEP-II cavity analysis is from the SFO1 post-processor applied to SUPERFISH rf cavity calculations.

The ten parallel cooling circuits with a 4.5 L/s total water flow rate are sufficient to keep the rise in water temperature to about 10°C, for a total power dissipation of 150 kW. With an inlet water temperature of 35°C assumed in the analysis, the average water temperature in the cooling channels is 40°C. The film heat transfer coefficient, h_f, on the surface of all cooling channels is evaluated using the Dittus-Boelter relation:

$$h_f D_H/k = 0.023\,\mathrm{Re}^{0.8}\,\mathrm{Pr}^{0.4} \qquad (2)$$

where D_H is the channel's equivalent hydraulic diameter, k is the thermal conductivity of the coolant, and Re and Pr are, respectively, the Reynolds and Prandtl numbers for the coolant. Generally, a water velocity between 3 and 6 m/s represents a good compromise between a high film heat-transfer coefficient, which increases with velocity, and an increase in erosion and cavitation, which occurs at very high velocities. A water velocity of 5 m/s is selected to ensure fully developed turbulent flow and a high h_f of 21.2 kW/m^2°C while leaving some margin below the maximum suitable velocity. Convective cooling on the outer surface of the cavity is neglected. The physical properties of OFHC copper used in the analysis are given in Table 3.

Figure 2 shows the results of the heat transfer analysis for the PEP-II cavity. The average temperature on the cavity interior surface is about 52°C, which results in a reduction of the

Table 3: Material Properties used in Stress Analysis

Material:	304 Stainless Steel	OFHC Copper
Thermal Conductivity (W/m°C)	16.0	390.8
Thermal Expansion Coefficient (/°C)	14.4×10^{-6}	17.0×10^{-6}
Specific Heat (J/g°C)	0.502	0.385
Density (kg/m^3)	8.03×10^{3}	8.94×10^{3}
Young's Modulus of Elasticity (MPa)	193.0×10^{3}	118.0×10^{3}
Poisson's Ratio	0.30	0.30
Yield Strength (annealed) (MPa)	207.0	69.0

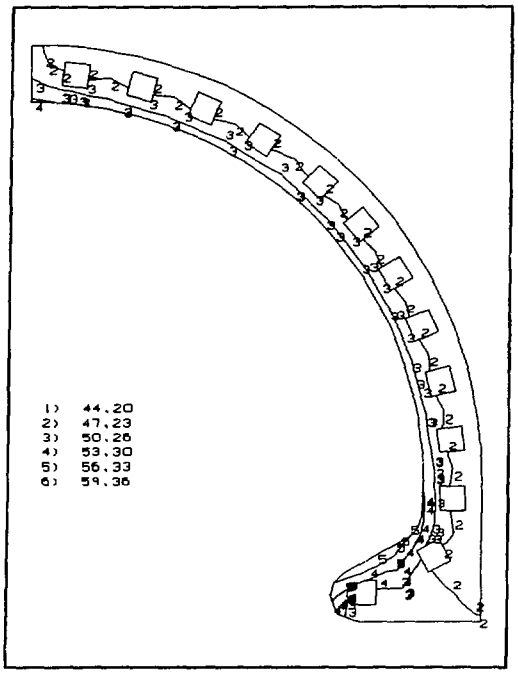

Figure 2: Temperature distribution (°C) for PEP-II cavity design with 150 kW power dissipation and 40°C average water temperature

cavity Q by 3.6% from the decrease in copper electrical conductivity with increasing temperature. The maximum surface temperature occurs on the outer part of the nose-cone, where the power flux in the 2-D rf calculation is greatest, but the value is still acceptable.

Once the heat transfer analysis is complete, the total mechanical and thermal stress on the cavity is determined. This stress analysis has two steps. In the first step, only the effects of atmospheric pressure on the cavity (vacuum loading) and water pressure in the cooling channels are considered. This is the cold cavity condition. In the second step, the effects of thermal expansion of the copper from rf heating is added to the vacuum loading and water pressure. This permits a separation of the external mechanical loads (water and vacuum) from thermal effects. Figures 3 and 4 show the contours of the equivalent von Mises stress, $\bar{\sigma}_e$, defined by:

$$\bar{\sigma}_e = \sqrt{[(\sigma_1 - \sigma_2)^2 + (\sigma_2 - \sigma_3)^2 + (\sigma_3 - \sigma_1)^2]/2} \tag{3}$$

where σ_1, σ_2, and σ_3 are the principal local stress components. Following the von Mises criterion, the copper yields (deforms inelastically) when $\bar{\sigma}_e = \sigma_y$, the yield strength.

Figure 3 shows that the internal stress from water pressure in the cooling channels and vacuum loading is less than 5 MPa. Compare this distribution with Figure 4, which shows the equivalent stress distribution for the PEP-II cavity at the maximum design power dissipation. With this cooling channel layout, the maximum equivalent stress is only 16 MPa, less than a quarter of the yield strength of fully annealed OFHC copper and well within a safe operating range. The highest stress point occurs at the outer radius of the central nose-cone, since this is the region with highest temperature gradients, causing

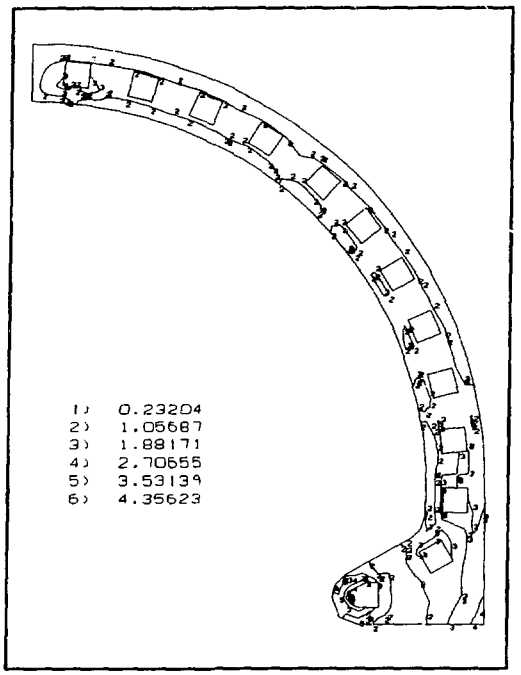

Figure 3: Equivalent stress on PEP-II cavity, including only vacuum loading and water pressure in cooling channels

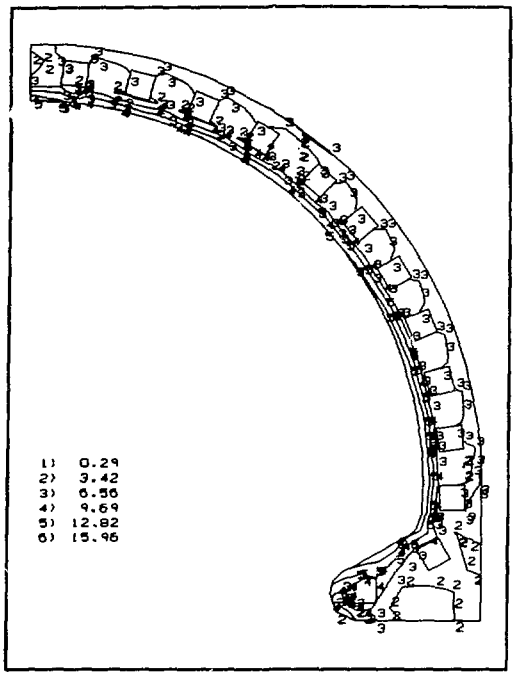

Figure 4: Equivalent stress distribution (MPa) for PEP-II cavity design with 150 kW power dissipation and 40°C average water temperature

differential thermal expansion.

Another result from the stress analysis is the total mechanical deformation of the cavity from all applied stress, shown with an exaggerated scale in Figure 5. The frequency shift caused by this deformation has been calculated to be -8 kHz from water pressure and vacuum loading alone, and -130 kHz total, including the thermal expansion. Most of the shift arises from the temperature change of the bulk copper, causing an overall increase in the cavity size. The expansion along the beam axis is mostly cancelled by an inward deformation caused by external atmospheric pressure on the cavity end walls.

Another design, with much thicker cavity walls, is also examined for a comparison of design trade-offs. The results of a heat-transfer and thermal-stress analysis of this design are shown in Figures 6 and 7. The differences in the results from the previous design with a 22 mm shell characterize the typical design trade-off that occurs: the thicker walls reduce the

deformation at the expense of increased internal stress. In this alternative design, the frequency shift from distortion is reduced to -102 kHz but the maximum equivalent stress increases to 25 MPa.

Nevertheless, on the basis of these 2-D computations, either design is suitable, since the maximum stress and frequency shift in both cases is acceptable. For PEP-II, the 22 mm shell design is the basis of the 3-D analysis. This design requires substantially less material and provides a higher margin for the internal stress, which is expected to be higher in the 3-D analysis when the effects of cavity wall openings and non-uniform heating are included.

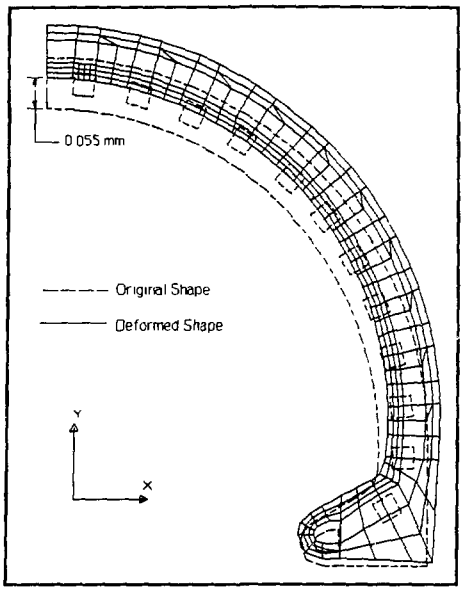

Figure 5: Exaggerated distortion of PEP-II cavity with 150 kW rf dissipation and vacuum loading

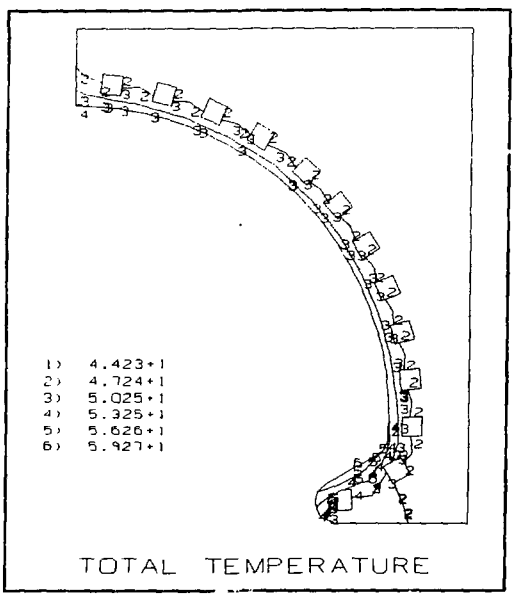

Figure 6: Temperature distribution (°C) for alternate PEP-II cavity design with 150 kW power dissipation and 40°C average water temperature

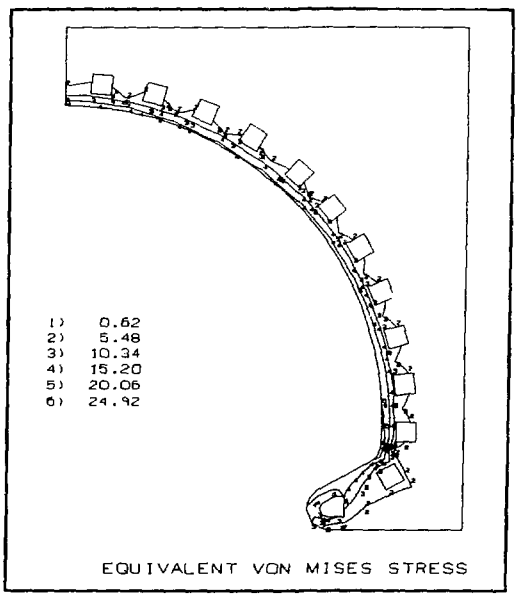

Figure 7: Equivalent stress distribution (MPa) for alternate PEP-II cavity design with 150 kW power dissipation and 40°C average water temperature

4. 3-D DESIGN ANALYSIS

4.1 PEP-II Cavity 3-D Finite-element Mesh

The 3-D design analysis begins with the creation of an appropriate finite-element mesh. The cavity has 3-fold rotational symmetry about the beam axis, the result of the three HOM waveguide ports placed at 120° positions around the axis. For the mechanical model, each identical 120° section can be further reduced to two 60° sections that have a reflection symmetry. To further reduce the size of the problem and the total number of mesh elements, the cavity is also treated as being symmetric about the central plane, perpendicular to the beam axis. Thus, the final part of the cavity modeled is 1/12 of a full cavity that has six waveguides, three on either side of the central plane.

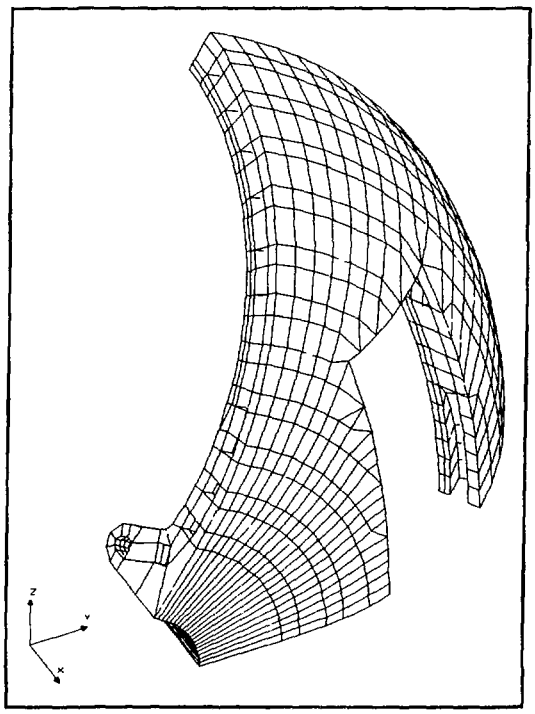

Figure 8: Finite-element mesh for cavity shell with internal cooling channels and no waveguide insert

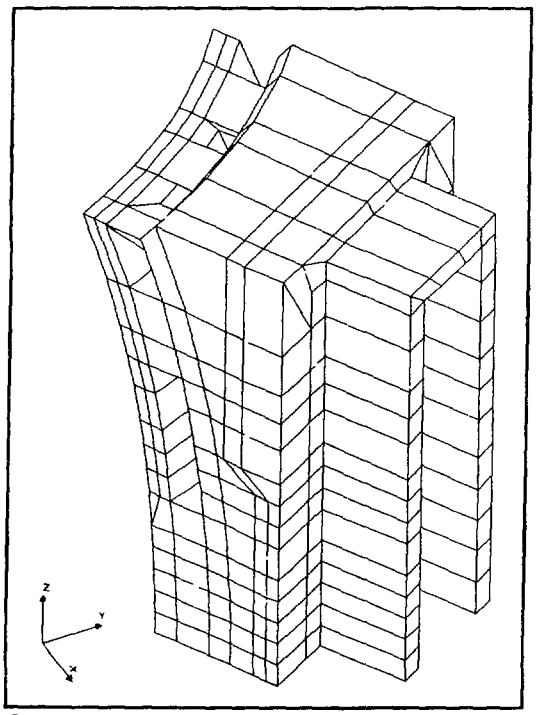

Figure 9: Details of the finite-element mesh for the waveguide insert with internal cooling channels

The finite-element model, generated using MENTAT, consists of 3206 nodes and 2018 eight-node, isoparametric, hexahedral elements. The mesh for the outer cavity shell, Figure 8, is produced by rotating a coarser version of the 2-D mesh shown in Figure 2 in 3° steps, from 0° to 60° about the beam axis (x-axis). A complete 3-D heat-transfer and thermal stress analysis using the coarser mesh before cutting the hole for the waveguide is performed. The results are compared with those of the 2-D analysis to ensure that no significant differences exist between the two meshes. Cooling channels, 10 mm square, are included throughout the shell.

Several mesh elements on the cavity wall are deleted, and the nodal coordinates of other elements changed to create an opening for a mesh of the waveguide iris insert, Figure 9. The insert mesh also includes several cooling channels. The resultant, final, mesh is shown in Figures 10 and 11 where the two sub-meshes have been merged. This mesh is used for all subsequent heat-transfer and thermal-stress analysis. The internal cooling channels are

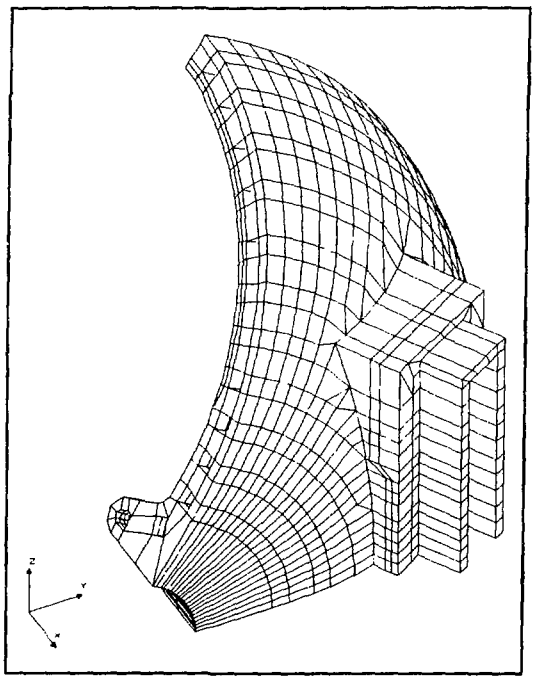

Figure 10: PEP-II cavity 3-dimensional finite-element mesh showing the cavity exterior surface

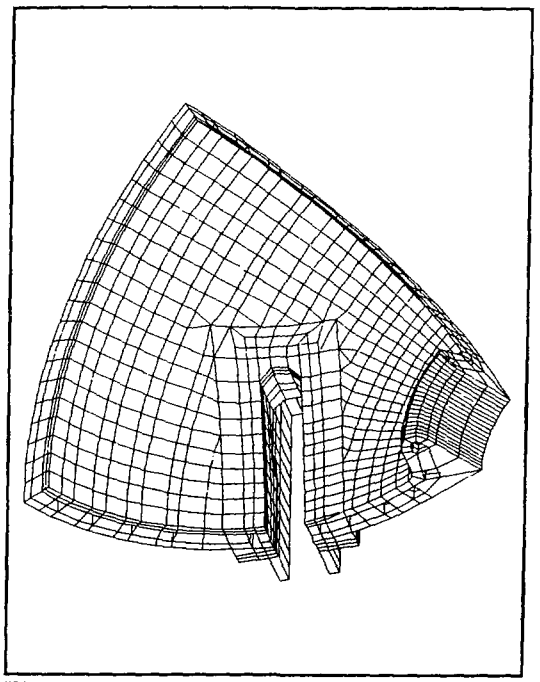

Figure 11: PEP-II cavity 3-dimensional finite-element mesh showing the cavity interior surface

represented by volumes inside the mesh where elements are not present, and film heat-transfer coefficients are assigned to the sides of elements surrounding these volumes. As in the 2-D analysis, the film coefficients are calculated using the Dittus-Boelter relation.

4.2 General Background for 3-D Analysis

4.2.1 RF Power Flux Distributions

ARGUS is the 3-D rf code used to generate the rf field distribution that is used for the stress calculations. As in the 2-D analysis, the power flux distribution is given by the rf computations. However, in the 3-D analysis this distribution is not conveniently available for use with the MARC finite-element code. The main problem is that the type of mesh used in the ARGUS 3-D rf codes is significantly different from the finite-element mesh used in the stress analysis. The rf code creates a mesh that consists of "bricks" or cells with edges parallel to the coordinate axes. As a result, the mesh describing a curved or sloped surface has many irregularities. The effects of this mesh surface roughness on the results of the computation can be reduced by using a finer mesh spacing, at the expense of additional computation time. A post-processor code for ARGUS calculates the power flux on the surface of each cell that is exposed on the interior of the cavity. As in the SUPERFISH post-processor, the surface conductivity of pure copper is used in the power calculations. A small computer program is used to interpolate the power flux data from the ARGUS results onto the interior surfaces of the finite-element mesh, and to prepare a suitable data file for the MARC finite-element code.

In addition, ARGUS can only take advantage of cavity geometrical symmetries that are reflections on planes perpendicular to the coordinate axes. Thus, the ARGUS mesh for the PEP-II cavity used to calculate the power flux distributions modelled one half of the cavity: the only cavity geometrical symmetry ARGUS can use is a reflection in a plane through the beam axis that passes through the centre of one waveguide iris. A useful consequence is that there are three distinct parts of the ARGUS mesh, each subtending 60° about the beam axis, that, for the fundamental cavity mode at 476 MHz, are modelled by the same finite-element mesh. This gives the opportunity to observe the sensitivity of the stress analysis to the rf mesh and interpolation code by performing stress analyses with power flux data from each distinct 60° segment in the rf calculation. To reduce the sensitivity of the stress analysis to

these possible rf mesh dependent effects, the reference rf power flux distribution is produced by averaging the flux distribution over all three segments.

4.2.2 3-D Stress Calculations

All 3-D heat-transfer and thermal stress calculations are performed using the MARC finite-element code, with MENTAT used as a pre-processor to prepare the input data and as a post-processor for viewing and plotting the results. The calculation for each case is broken into three steps: a heat-transfer calculation, a stress calculation on the cold cavity (with no input power flux) and a stress calculation with the thermal effects included.

The heat-transfer case is solved using the rf power flux distribution from ARGUS interpolated onto the finite-element surface mesh. This assumes no heat transfer through the symmetry planes of the finite-element model. The water channels are modelled by specifying the film heat-transfer coefficients on element surfaces bounding the water channel and by specifying a bulk temperature of the cooling water. The thermal conductivities of materials used in the cavity are also specified in this step. The temperature differences are assumed to be sufficiently small in the solution that the variation in thermal conductivity and film heat-transfer coefficients may be neglected. A simple linear heat-transfer analysis can then be used with this assumption.

As in the 2-D case, the first stress calculation considers only the effects of vacuum loading and water pressure in the cooling channels. The initial cavity temperature is assumed to be 35°C when no rf power is dissipated. This serves as a reference for the stress distribution from non-thermal sources. The second stress calculation includes not only the effects of vacuum loading and water channel pressure, but also the distortion and stress produced by the thermal expansion of the cavity materials where the thermal distribution computed in the heat-transfer calculation is used. The differences in stress at any location between the two stress calculations are those due solely to thermal effects. In both stress calculations, the symmetry of the problem requires that those nodes on the symmetry planes can only have displacements in those planes.

A range of cases are examined to find those aspects of the cavity mechanical design that have the greatest influence on the maximum stress. The final mechanical design must ensure that

the regions of maximum stress are within acceptable design limits for the materials being considered.

Consistently, the region of highest stress is at the ends of the waveguide iris. This occurs under external loading alone, vacuum and water pressure, as well as when thermal effects are included. Thus the element with highest equivalent stress is located at the end of the iris on the inner surface of the cavity. For this element, the equivalent stress and principal stress components at one of the internal Gaussian integration points are given in Table 4 for comparison between cases. An important conclusion from the principal stress component values is that, in all cases, there are only compressive stresses on this element.

4.3 Reference Case

The Reference Case consists of a heat-transfer and thermal-stress analysis performed using the mesh shown in Figures 8 through 11, assuming the entire cavity is fabricated from OFHC copper, an average water temperature of 40°C, a film heat-transfer coefficient of 21.2 kW/cm^2°C corresponding to 5 m/s water velocity, and an ARGUS power-flux distribution, averaged over the three symmetric segments. The copper properties and film coefficient are identical to those used in the 2-D analysis. Figure 12 shows the power-flux distribution used in the calculation. It is clear that there is a significant region of very high power flux near the end of the iris on the waveguide side closest to the beam. Figures 13, 14 and 15 show results from the heat-transfer and thermal-stress calculations. As expected, the temperature distribution on the inner surface is very similar to the power flux distribution. Although the temperature (see Figure 13) is highest near the end of the iris, the maximum, 89.5°C, is well within acceptable limits for the cavity vacuum. The stress results (see Figure 14) are of greater concern. The maximum stress occurs at the end of the iris and, in this calculation, slightly exceeds the yield stress for OFHC copper. Figure 15 shows the temperature and stress distribution on the inner surface in the iris region in greater detail. The maximum stress value in plot differs from that in Table 4 because the surface stress is extrapolated from the values at element interior integration points, one of which is used in the table.

Table 4: Stress at Element #1149, located at the end of the iris next to cavity wall

Case Description	Equivalent von Mises Stress (MPa)			Principal Stress (MPa)		
	External	Thermal	Total	Minimum	Middle	Maximum
Reference	11.0	54.2	65.2	-81.6	-31.4	-7.9
1) Cooling on Outer Waveguide Edge	11.0	55.2	66.2	-82.6	-31.8	-7.7
2) Waveguide Cooling near Cavity Wall	11.0	54.3	65.3	-81.2	-30.8	-7.5
3) Stiffer Copper End-piece for Waveguide	10.6	52.6	63.2	-79.3	-30.9	-7.8
4) Steel End-piece for Waveguide	10.8	52.3	63.1	-78.9	-30.4	-7.6
5) Steel Waveguide Outer Shell	10.5	51.8	62.3	-78.0	-30.3	-7.5
6) Reduction in Water Velocity	11.0	56.7	67.7	-84.5	-32.2	-8.0
7) Removal of Local Iris Hot Spot	11.0	50.4	61.4	-77.0	-30.0	-7.6
8) Stiffer Copper Outer Cavity Shell	9.3	57.9	67.2	-84.2	-32.3	-8.2
9) Steel Outer Cavity Shell	10.2	58.7	68.9	-86.1	-32.6	-8.3
10) Rigid End Flange on Waveguide	7.7	64.1	71.8	-89.7	-33.0	-9.0
11) Stiff Shell Between Waveguide	10.3	54.5	64.8	-81.3	-31.7	-8.1
12) Water Temperature Distribution	11.0	50.6	61.6	-77.6	-30.2	-8.0
13) Small Stiff Shell between Waveguide	10.4	53.6	64.0	-80.4	-31.5	-8.0
14) Stiffer Waveguide End and Outer Shell	8.8	51.3	60.1	-76.1	-30.9	-7.9
15) Coolest Water on Waveguide Insert	11.0	44.3	55.3	-70.1	-28.9	-7.2
16) Optimum Design Configuration	9.3	40.0	49.3	-63.2	-28.0	-7.0

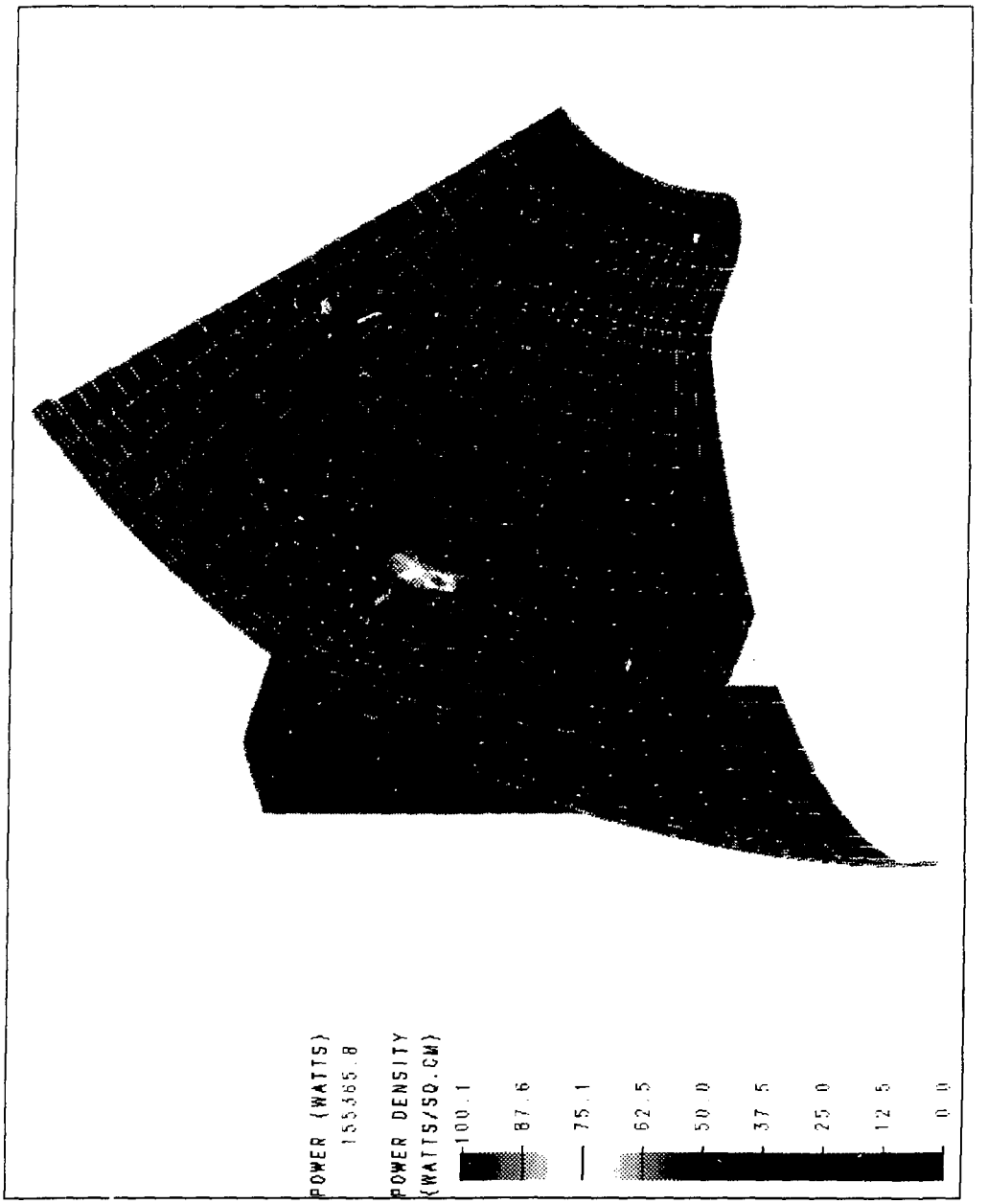

Figure 12: ARGUS power-flux distribution averaged over 3 symmetric 60° segments

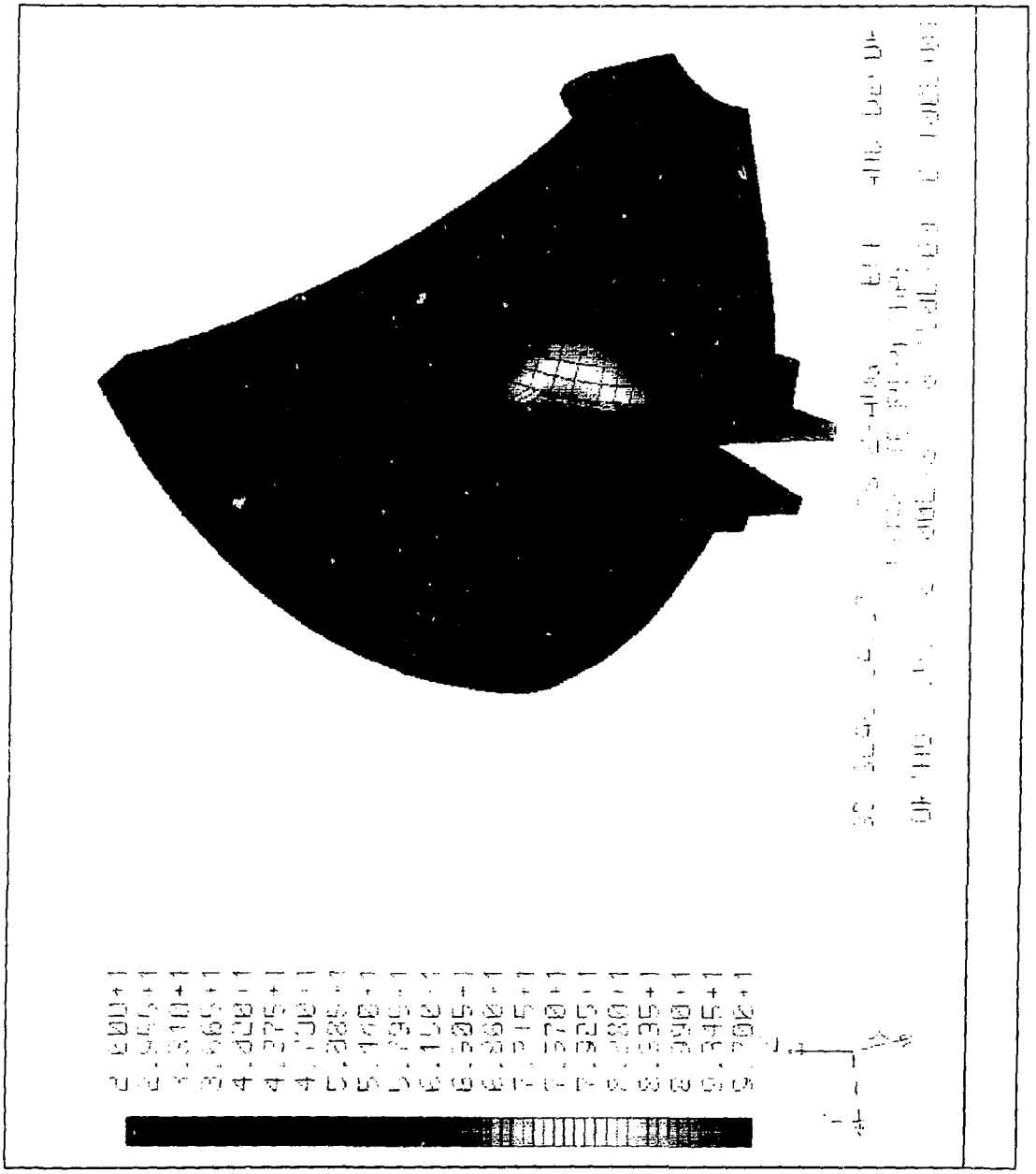

Figure 13: Calculated temperature (°C) on inner cavity surface for the reference case

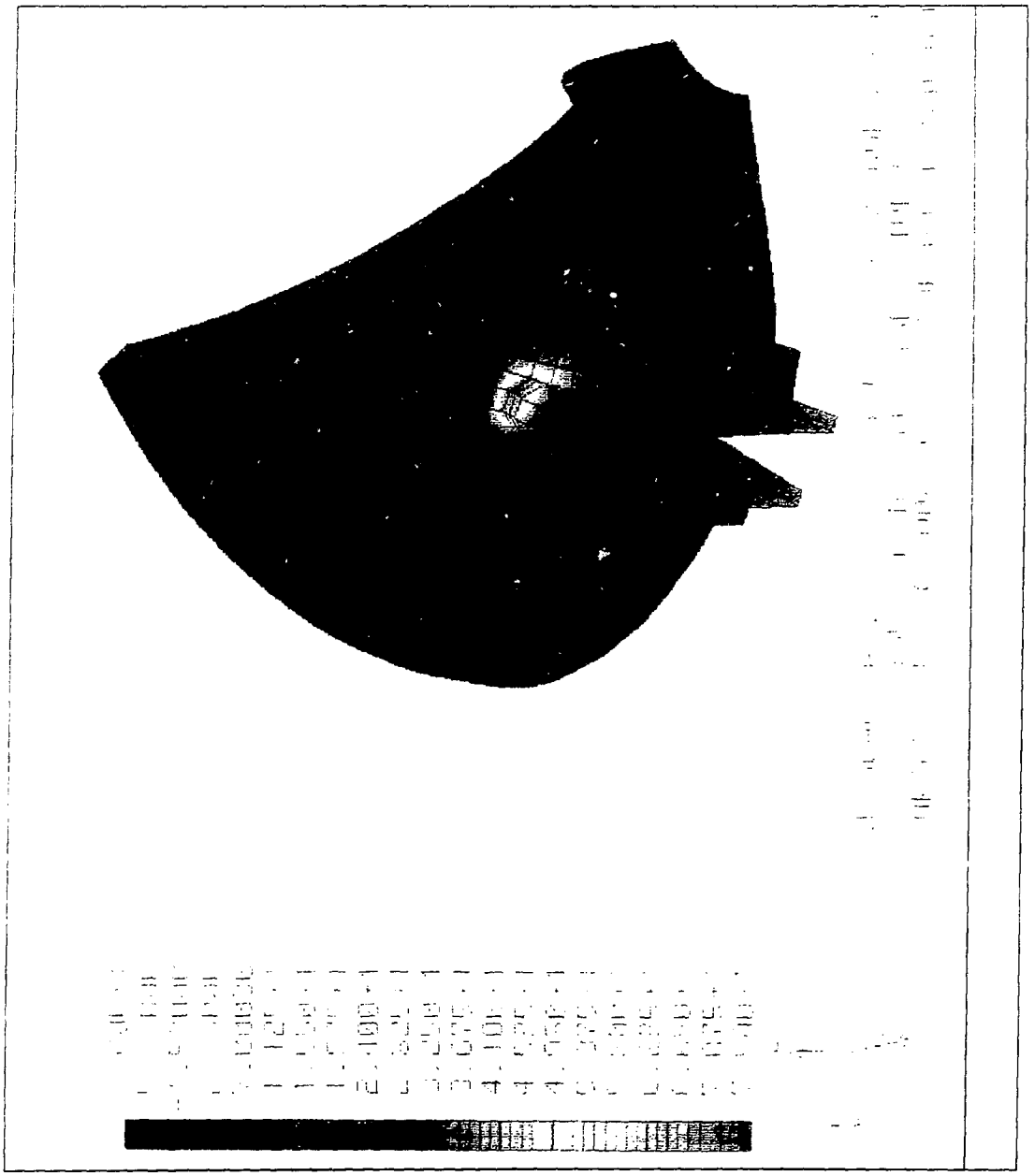

Figure 14: Calculated equivalent stress (MPa) on inner cavity surface for the reference case

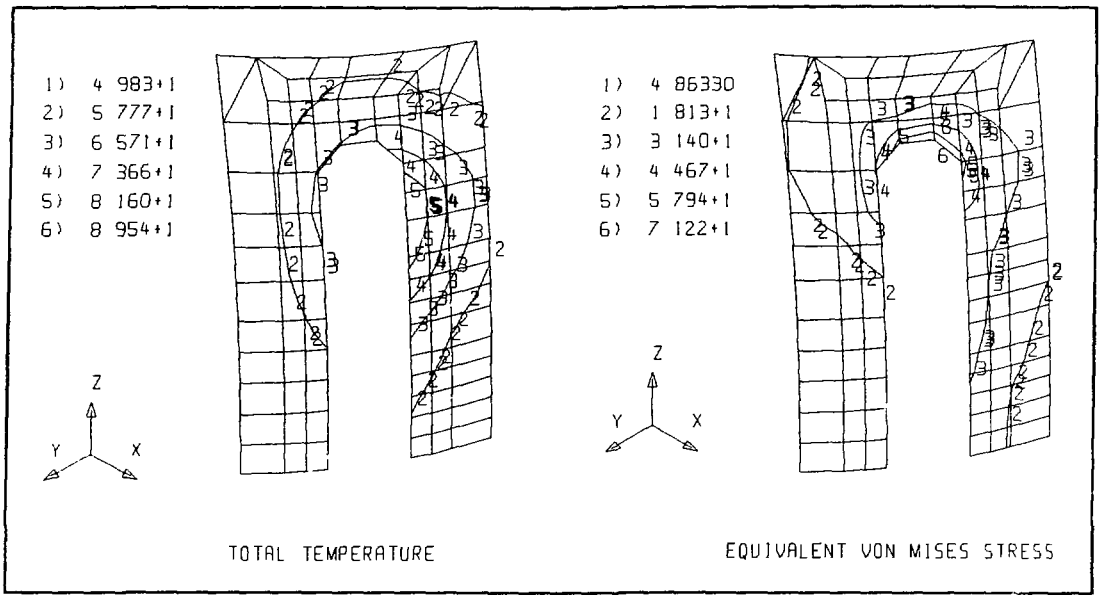

Figure 15: Temperature distribution (°C) and von Mises equivalent stress (MPa) in the interior iris region for the average heat flux distribution extracted from the ARGUS data

4.4 Test Cases

In this section the results of various different stress calculations are examined. Most cases are variations either in the cooling parameters (e.g., film heat-transfer coefficients or water temperature) or in the mechanical properties of the model (e.g., Young's modulus or material used for some elements). For convenience, these parameters are occasionally varied to approximate changes in the dimensions of the mechanical model, as rebuilding a new mesh with modified nodal coordinates is much more time-consuming. In most cases, the region of the finite-element model affected is illustrated. A brief interpretation of the result of each case is also given.

4.4.1 Case 1: Extra Cooling on Outer Waveguide Edge

Extra cooling on the outer waveguide edge is simulated using the same film heat-transfer coefficient that is used in the cooling channels on the outside of the outer waveguide section, shown in the shaded area in Figure 16. Additional cooling channels would be added in this section in an actual cavity. The effectiveness of this additional cooling for reducing the iris

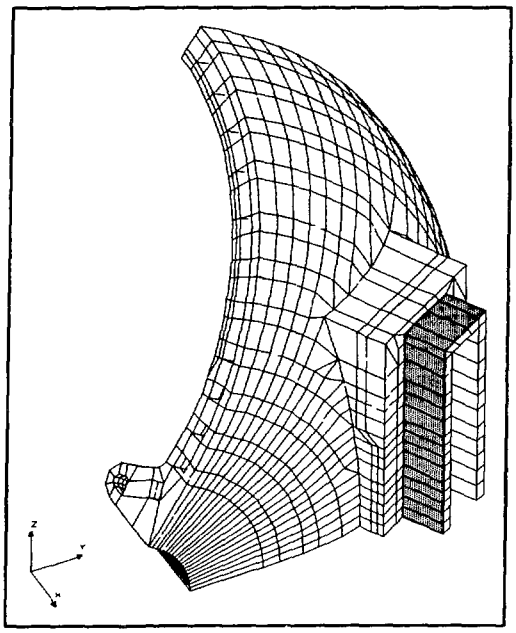

Figure 16: Mesh for Case 1, showing shaded region where additional cooling was added to outer edge of waveguide

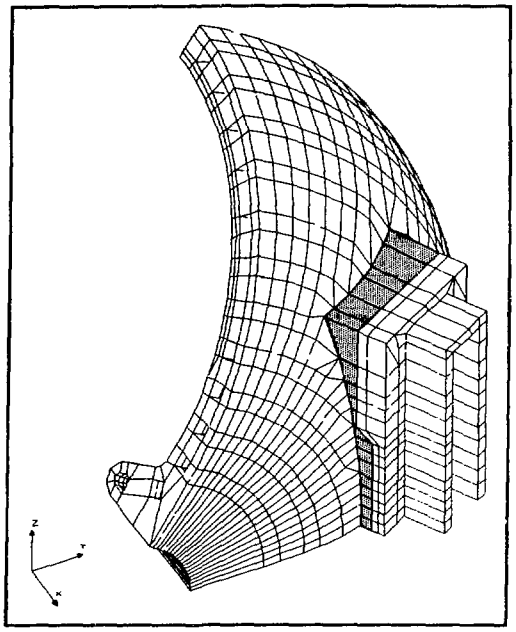

Figure 17: Mesh for Case 2, showing shaded region of additional cooling closer to cavity wall

stress is non-existent. Instead, the increased cooling on this part of the waveguide results in less thermal expansion than the adjacent iris region and produces an increase in the maximum stress of 1 MPa.

4.4.2 Case 2: Extra Waveguide Cooling Close to Cavity Wall

As in Case 1, additional cooling of the waveguide area was simulated using non-zero film-heat-transfer coefficients on the outer surfaces of waveguide elements close to the cavity wall, as shown in Figure 17. This cooling closer to the inner cavity surface is like adding a second layer of cooling channels outside the inner water channel layer. The maximum surface temperature in the iris region is reduced by 2°C, but the stress is very slightly increased by 0.1 MPa, a negligible amount. This indicates that the first, inner layer of water cooling channels is very effective, and additional water cooling outside is ineffective.

4.4.3 Case 3: Stiffer Copper End-piece for Waveguide

In this case, a stiffer copper end-piece for the waveguide (indicated by the shaded region in Figure 18) is used to provide reinforcing in the iris end region. The additional stiffness is simulated by increasing the Young's modulus of those elements by a factor of 3. This is approximately equivalent to increasing the copper thickness of this region by 50%. As expected, the strengthening of the end region reduces the maximum stress in both situations: by 0.4 MPa with just vacuum and water pressure, and by 2 MPa when thermal stress is added. However, both decreases are small, less than 4%.

4.4.4 Case 4: Steel End-piece for Waveguide

Since a stiffer copper end-piece results in a significant, albeit small, decrease in the maximum stress, Case 4 is a more realistic situation, where the material properties of 304 stainless steel are used for the end-piece region. The reduced thermal conductivity of the

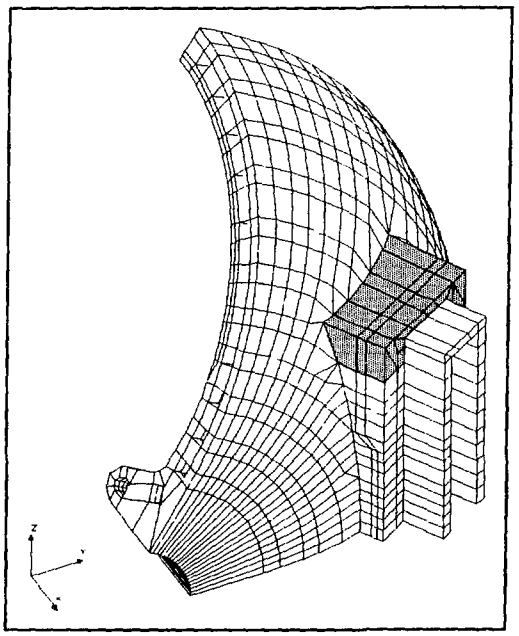

Figure 18: Mesh for Case 3 and 4, where shaded region indicates the stiffened end-piece

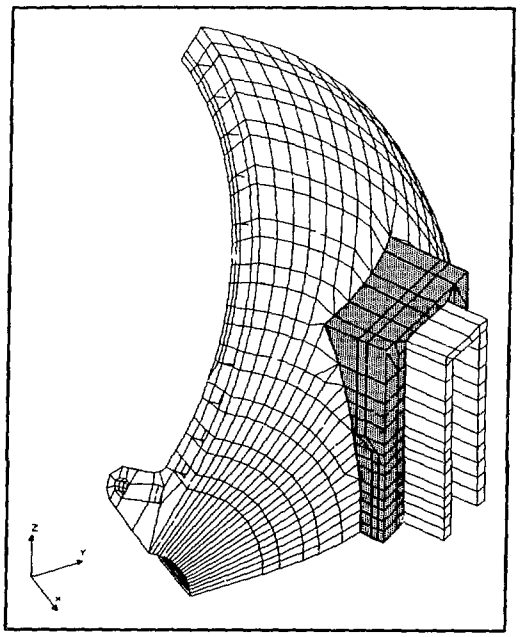

Figure 19: Mesh for Case 5, where shaded region indicates 304 stainless steel outer waveguide shell

steel is not significant, since there is no external power flux through the material. The maximum stress reductions are similar to those in Case 3: 0.2 MPa under external loads and 2.1 MPa when thermal effects are included. The maximum temperature in the iris region differs from Case 3 by less than 0.5°C.

4.4.5 Case 5: Steel Waveguide Outer Shell

Case 5 examines the stress reduction that would occur if the entire outer shell of the waveguide section were made from 304 stainless steel. This results in a stiffer outer structure all around the entire iris. The reductions are greater than Case 3 or 4, but not large: 0.5 MPa reduction without thermal effects and 2.9 MPa overall reduction when thermal effects are added. Although these potential reductions are useful, the maximum stress remains close to the yield stress of OFHC copper. The conclusion from Cases 3 to 5 is that a steel outer shell will be useful, but other design changes must be used to achieve greater stress reductions.

4.4.6 Case 6: Reduction in Water Velocity

Although water velocities of 3 to 6 m/s are generally considered acceptable for good heat transfer without severe erosion problems, other design guidelines may apply as well. One other criteria is that the Reynolds number of the coolant should not exceed 50 000, again to avoid cavitation and excessive erosion. For the large cooling channel size used (100 mm^2), this value occurs at a velocity of only 3.7 m/s. Case 6 examines the consequences of reducing the water velocity to this value and the corresponding reduction of the film heat-transfer coefficient to 16.5 $kW/m^2°C$. Despite the 25% drop in the film coefficient, the maximum temperature increase is less than 10%, from 89°C to 93°C, and the maximum stress rises by only 2.5 MPa, less than a 4% change. This is reassuring for production operation of the cavity, since it indicates that this design is relatively insensitive to fluctuations or changes in water pressure and velocity.

4.4.7 Case 7: Removal of Local Iris Hot Spot

The highest power flux in the iris region is over 90 W/cm^2, compared to an average flux of only 15-25 W/cm^2 further away. The flux through the surface of 12 elements with the

highest flux in this region was set to between 35.5 and 37.5 W/cm^2, the average flux value on the adjacent elements. This reduction approximates the elimination of the "hot spot" to see whether the high stress is primarily caused by the localized heating. As expected, there is a significant maximum surface temperature drop, about 10°C, which is a 20% reduction of the surface temperature change with heating. However, the maximum stress is reduced by only 6% to 61.4 MPa. This indicates that the overall temperature distribution in the cavity is a greater contributor to the high stress than the localized iris heating.

4.4.8 Case 8: Stiffer Copper Outer Cavity Shell

An overall deformation of the cavity shell is one way the temperature distribution can produce local high-stress concentrations, especially in long slots like the iris aperture. One possible way to reduce this stress would be to reduce the deformation by stiffening the cavity shell. To test this approach the outer cavity shell, shown in Figure 20, is stiffened using a value 3 times that of OFHC copper for the Young's modulus of the shell material. All other mechanical properties of the shell are assumed to be the same as copper. As in Case 3, this is approximately equivalent to using an outer copper shell 50% thicker. The result is disappointing. The maximum stress with just water pressure and vacuum loading is decreased by 1.7 MPa. However, the maximum stress with the power flux is increased by 2.5 MPa. In effect, the maximum thermally induced stress increases by over 4 MPa. This mirrors the results of the 2-D calculations as well, where increasing the thickness of the outer shell also increased the thermal stress, while reducing deformation.

4.4.9 Case 9: Stainless Steel Outer Cavity Shell

Another possible material for the outer cavity shell is 304 stainless steel. It has a higher Young's modulus, so it also reduces the total cavity deformation when used as the outer shell. Case 9 uses the same elements to define the outer shell (see Figure 20) as those in Case 8, but the thermal and mechanical element properties are those of 304 stainless steel. The result is quite similar: a reduction of the maximum stress by 0.8 MPa with just water pressure and vacuum loading, but an increase by 3.7 MPa when thermal effects are included. These two cases indicate that a stiffer or thicker outer shell is not useful for stress reduction and that the shell should only be thick enough to handle the vacuum and water pressure loads.

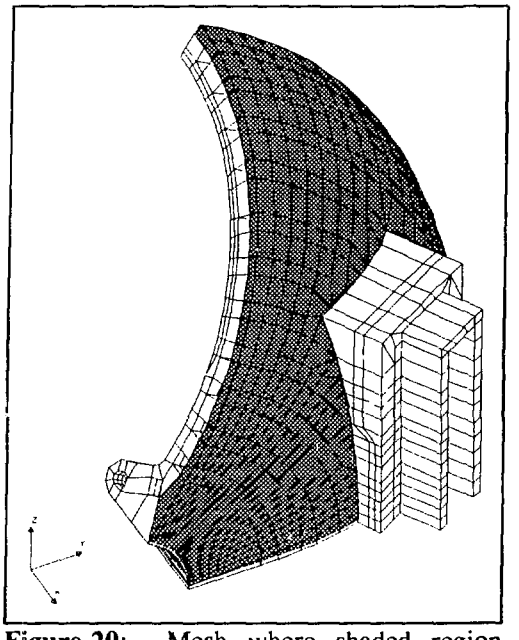

Figure 20: Mesh where shaded region indicates thicker copper (Case 8) or stainless steel (Case 9) outer cavity shell

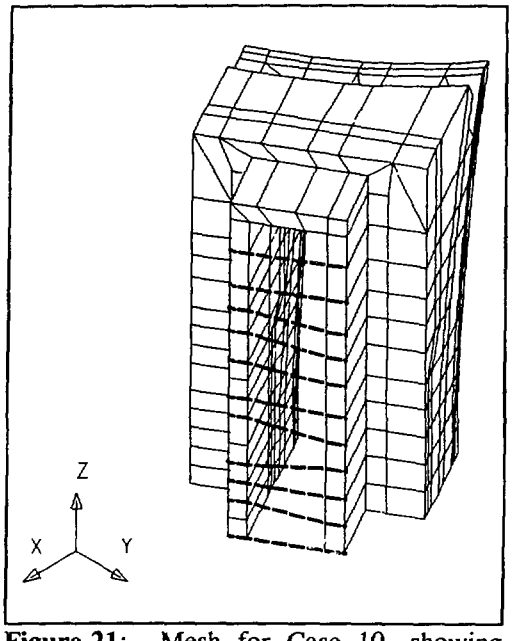

Figure 21: Mesh for Case 10, showing "tying" constraints applied to the waveguide end

4.4.10 Case 10: Rigid End Flange on Waveguide

The end of the waveguide away from the cavity will have a thick flange, where the HOM damper will be mounted. This flange also reduces the deformation that can occur under high-power operation. The effects of a rigid flange mounted on the waveguide end can be simulated in the finite-element code by applying appropriate boundary conditions on the end nodes that fix the relative positions of all nodes in the end plane in all but the z-direction. The "tying" constraints are shown in Figure 21. These boundary conditions are probably a worst-case analysis, since a real flange still has some distortion. The results indicate the same trend as the two previous cases. There is a 30% drop in the maximum stress when only vacuum and water pressure are considered, but a 10% increase in maximum stress when thermal loading is added. The net contribution to the stress from thermal effects increases by 10 MPa. The conclusion here is that the flange should be located far from the cavity wall, if feasible. The HOM dampers add additional mechanical stress to the waveguide iris, and must have mechanical support in addition to the cavity.

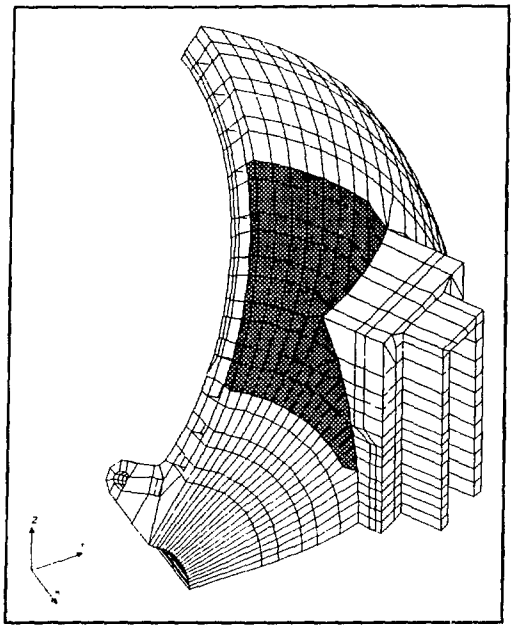

Figure 22: Mesh for Case 11, where shaded region indicates thicker OFHC copper on part of the outer cavity shell

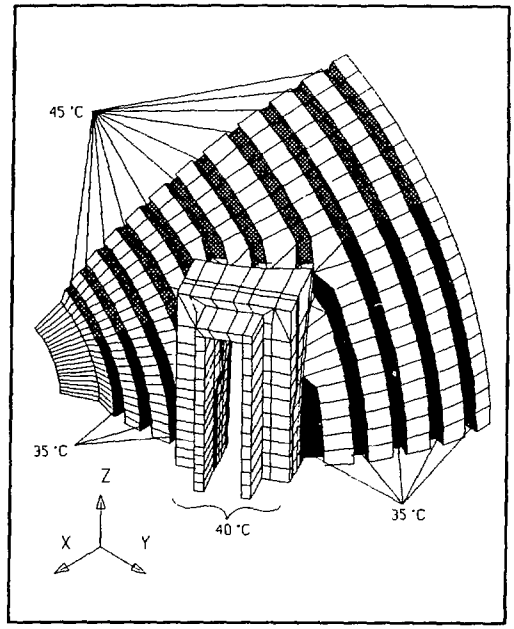

Figure 23: Case 12 cooling temperature distribution in cavity shell: 35°C in dark area, 40°C in waveguide, 45°C in light area

4.4.11 Case 11: Stiff Outer Shell between Waveguide

Although a stiffer outer shell over the entire cavity causes an increase in the maximum stress, cases 3 to 5 show that additional stiffness around the ends of the waveguide iris does reduce the stress. In Case 11, additional stiffness is added to the outer shell between the waveguide iris ends, Figure 22, to see whether this produces a similar improvement. Again, the Young's modulus of the copper in this part is increased by a factor of 3 to simulate a 50% thicker outer shell. The result shows a slight overall improvement in the maximum stress, a reduction of 0.4 MPa, but a closer examination shows that all the improvement is in a reduction of the stress produced by the external loads of water and atmospheric pressure. The portion attributable to thermal effects actually increases by 0.3 MPa.

4.4.12 Case 12: Water Temperature Distribution

The Reference Case and cases 1 to 11 all use a constant, average water temperature of 40°C throughout the cooling channels. Case 12 tests the significance of this assumption by using the temperature distribution shown in Figure 23, where 35°C water is used in the cavity sector containing the waveguide, 40°C is used in the waveguide iris insert and 45°C is used in the sector between the waveguide. Despite the somewhat unrealistic temperature distribution, this case gives an indication of the sensitivity of the maximum stress to the cooling channel layout. The result is a stress reduction equal to Case 7, indicating that the effect of the local high-power flux can possibly be reduced by paying careful attention to smaller overall temperature variations during the detailed design.

4.4.13 Case 13: Small Stiff Outer Shell between Waveguide

This case is similar to Case 11, except that the region where the outer shell is stiffened is reduced to include only that part between the ends of the waveguide inserts, as shown in Figure 24. Again, the Young's modulus of copper in this region is increased by a factor of 3 to simulate a 50% thicker outer shell. The result is a reduction of maximum stress by 1.2 MPa, with a 0.6 MPa reduction in the contribution from thermal effects. This is a very modest reduction, but it indicates that reinforcing or stiffening in this region is useful, compared with stiffening the entire outer shell.

4.4.14 Case 14: Stiffer Waveguide End and Outer Shell

This case is a combination of Case 3 and 13, where both the waveguide ends and the cavity outer shell between them, as shown in Figure 25, is stiffened by increasing the Young's modulus of the copper by a factor of 10. This is approximately equivalent to increasing the copper thickness by a factor of 2. The result is a decrease in the maximum stress by 5.1 MPa overall, and a decrease of 2.9 Mpa caused by thermal effects alone. This is encouraging, because it indicates that, to some extent, the incremental improvements of each of the cases are additive.

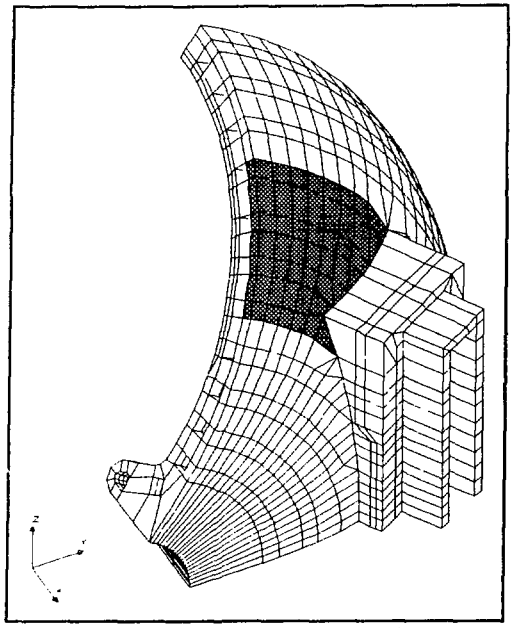

Figure 24: Mesh for Case 13, where shaded region indicates thicker OFHC copper on outer cavity shell

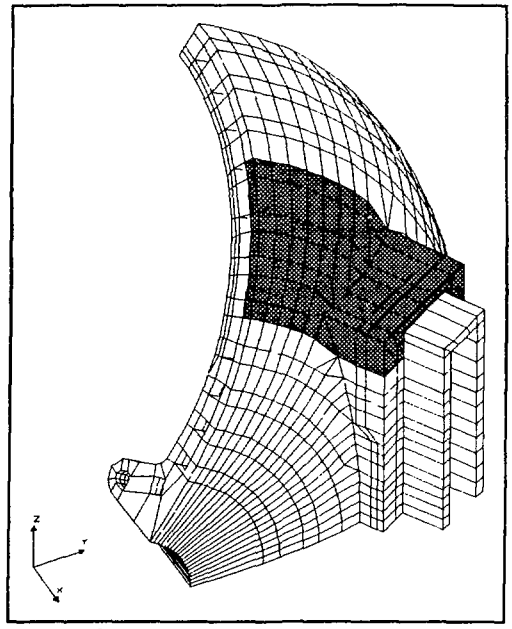

Figure 25: Mesh for Case 14, where shaded region indicates thicker OFHC copper on cavity shell and waveguide insert

4.4.15 Case 15: Coolest Water on Waveguide Insert

The stress reduction in Case 12, where the warmest water is between the waveguide inserts, is a clue that the major contributor to high thermal stress may be the azimuthal variation in the shell temperature near the iris radius. Assuming that this is true, an optimum cooling water temperature distribution would reduce this variation as much as possible. Case 15 is a test of this hypothesis where the water temperature around the waveguide insert is 35°C (the water inlet temperature), and the rest of the cavity water is at 45°C. This distribution causes a reduction in maximum stress by 10 MPa: 15% of the overall stress and 20% of the thermal stress contribution. This is a clear indication that on the final cavity design the inlets for the cooling water should be on the waveguide inserts.

4.4.16 Case 16: Optimum Design Configuration

This final test case uses all the design changes from previous cases that appear to be beneficial in reducing the maximum stress. In this regard, the results of Case 5, 14 and 15 lead to the Case 16 configuration shown in Figure 26. 304 stainless steel is used for the outer shell of the waveguide insert and on the cavity outer shell between the waveguide ends. Thicker steel for the waveguide insert ends and part of the outer shell is simulated using a Young's modulus for these sections that is 3 times the value for steel. The coolest water, at 35°C, is used around the waveguide inserts; warmer water, 40°C, circulates at larger and smaller radii than the inserts; and the warmest water, 45°C, is used between the ends of the inserts. This could be achieved by having the cooling water inlets at the inserts, then circulating the water to larger and smaller radii before reaching water outlets between the inserts.

The changes result in a substantial drop in the maximum stress from 65.2 MPa to 49.3 MPa, and the contribution from thermal effects drops from 54.2 MPa to 40.0 MPa. This occurs even though the maximum surface temperature only drops 1°C! The final surface temperature and von Mises stress distributions in the iris region are shown in Figure 27. These distributions should be compared to those in Figure 15 for the Reference Case. The results clearly indicate the care required when considering the actual water temperature distribution and the location of mechanical reinforcing in the design analysis. The results of this case are used in determining details of

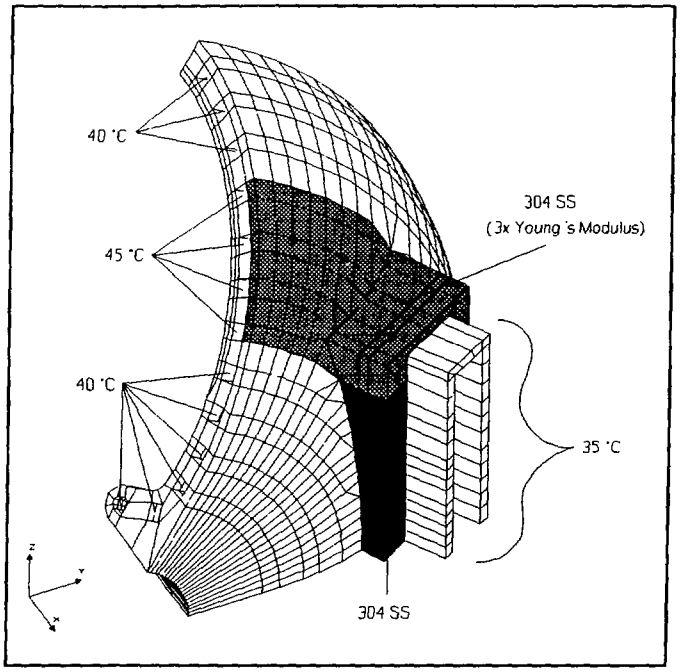

Figure 26: Mesh for Case 16, showing cooling water temperature distribution and 304 stainless steel on waveguide inserts and part of outer cavity shell

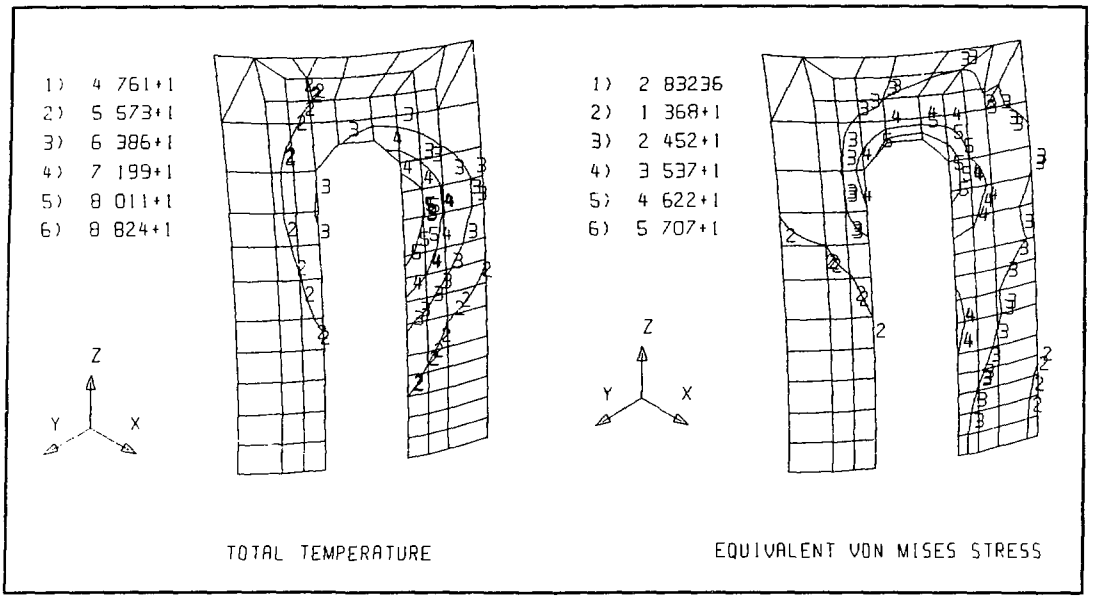

Figure 27: Temperature distribution (°C) and von Mises equivalent stress (MPa) in the interior iris region for Case 16

the proposed cavity mechanical design.

4.5 Conclusions from Stress Analysis

Now the results of the stress analysis from the optimum design are compared to the mechanical design criteria for good engineering practice. Considering both static and cyclic loading (fatigue failure) of the cavity structure, the design stress limits are as follows:

Static loading: Normally, in the case of a self-limiting load such as thermal strain-induced stress, a total load between σ_y and $2\sigma_y$ will cause plastic deformation during the first loading cycle. Removal of the load leaves some built-in residual stresses, such that any subsequent application of the same load only causes elastic deformation in the structure.

From a structural point of view, this is allowed in design codes such as the ASME Boiler and Pressure Vessel Code [6], where the thermal stress is classified as Q and the limit for the total load, thermal and mechanical, is $2\sigma_y$ for OFHC copper, to

produce a design that is practical but still safe. The maximum stress permissible from external loads (i.e., water pressure and vacuum loading) is $0.67\sigma_y$. The total stress from external loads is less than 11 MPa for all cases, which is much less than the ~45 MPa limit for copper. Since the high stress is localized at the end of the waveguide, the area that would undergo plastic deformation during the first cycle is very small and should not disturb the rf characteristics of the structure in a significant manner.

Cyclic loading: Since the highest stress is in compression, any yielding in the first cycle produces some tensile internal stress. Subsequently, during a typical cycle, the mean stress, $\sigma_m = (\sigma_{max} + \sigma_{min})/2$, is in compression. For $\sigma_m \leq 0$, the limit of the alternating stress, $\sigma_a = (\sigma_{max} - \sigma_{min})/2$, on a typical Goodman's diagram for fatigue life, is equal to the endurance limit of the material (see [7]). The endurance limit for OFHC copper, based on 10^6 cycle, is ~70 MPa [8] (about the same as its yield strength). The predicted σ_a for the PEP-II cavity is only slightly higher than 1/2 σ_y. This shows there is a good design margin using OFHC copper.

From the above discussion concerning the safe design limits, OFHC copper is suitable for the entire structure (except where 304 stainless steel is chosen for other reasons). This facilitates the fabrication process quite a bit, because there is so much experience with OFHC copper compared to most of the high-strength copper-based materials.

5. PROPOSED CAVITY DESIGN AND FABRICATION

5.1 Introduction

The high-power rf cavities should be manufactured from OFHC copper, with 304 stainless steel cladding over all waveguide inserts and large ports. In addition to the three HOM damper waveguide connects, there are three other major ports on the equator of the cavity: a 263 mm port to accommodate a PEP coaxial drive loop, a small port to accommodate an existing tuning plunger (from a PEP cavity), and a 50 mm by 200 mm racetrack port that can be used as an alternative iris-coupled rf drive port. Three small 25 mm ports are also shown for miscellaneous diagnostic ports.

Figure 28 shows an assembly view of the entire cavity. In this design the toroidal shell comprises four sections:

- a main cavity inner vacuum and rf shell, Figure 29, with cooling channels machined into its outer surface and a two-piece outer shell, Figures 30 and 31, to cover the cooling channels;
- a smaller cavity inner vacuum and rf lid, Figure 32, with its associated outer shell, Figure 33; and
- two beam port assemblies with embedded cooling channels, Figure 34.

All sections have joints parallel to the equator (perpendicular to the beam-axis). Waveguide inserts (Figure 35), rf coaxial-drive-loop port (Figure 36), tuner port (Figure 37), and rf iris-drive port (Figure 38), are machined with separate cooling channels for each part. Brazing is the preferred joining technique, with simple braze-joint geometries, to ensure the required dimensional tolerances. Brazing the cavity takes several steps, including intermediate leak testing, and rf tuning of the cavity precedes final assembly.

The prototype cavity is machined from rough forgings to minimize setup changes, while the production cavities use precision forgings and are finished in the same manner as the prototype cavity.

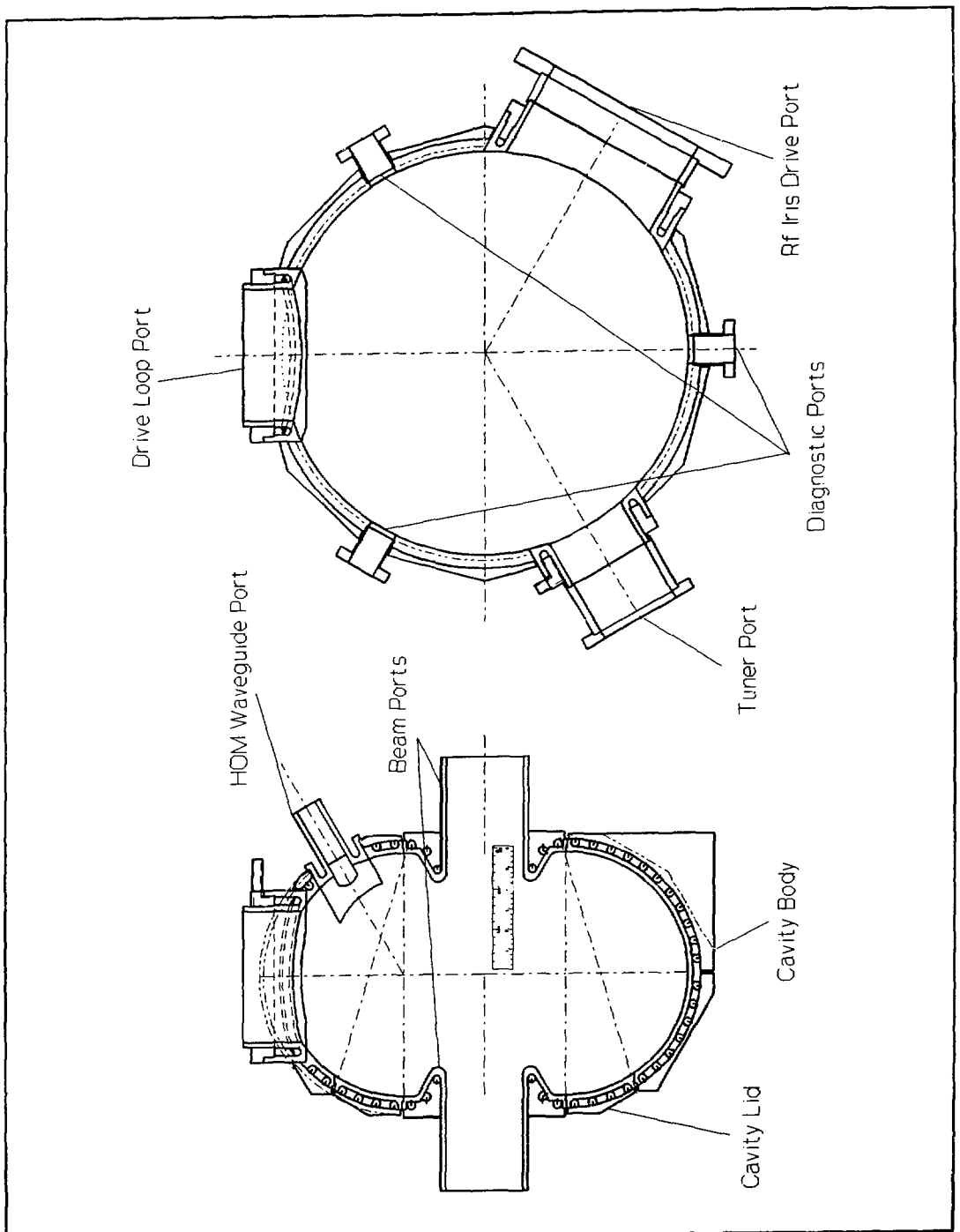

Figure 28: Assembly view of proposed PEP-II cavity

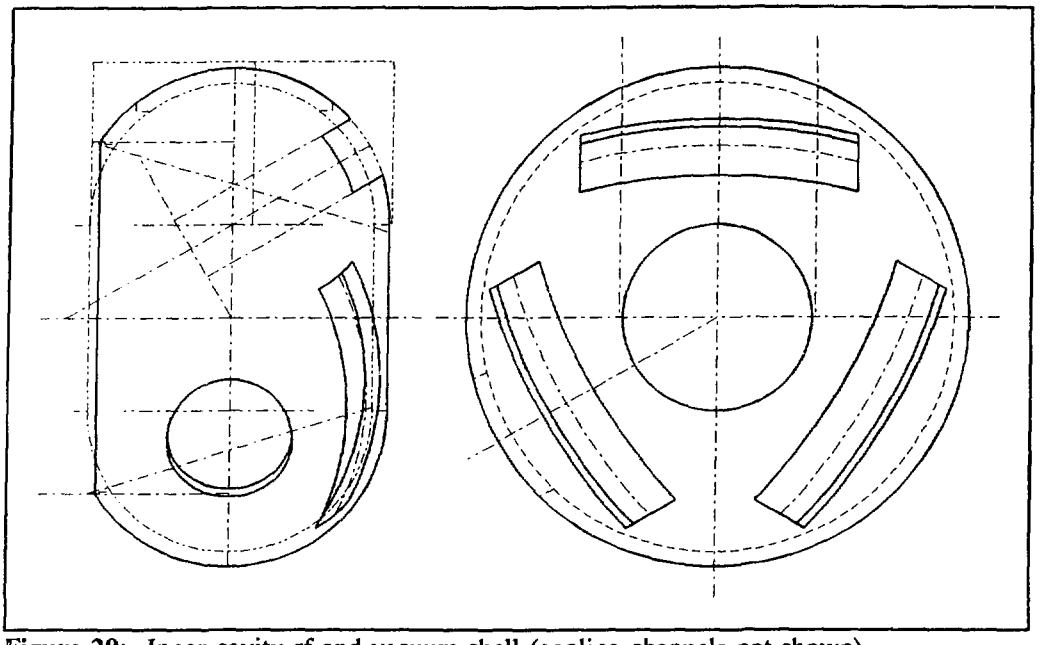

Figure 29: Inner cavity rf and vacuum shell (cooling channels not shown)

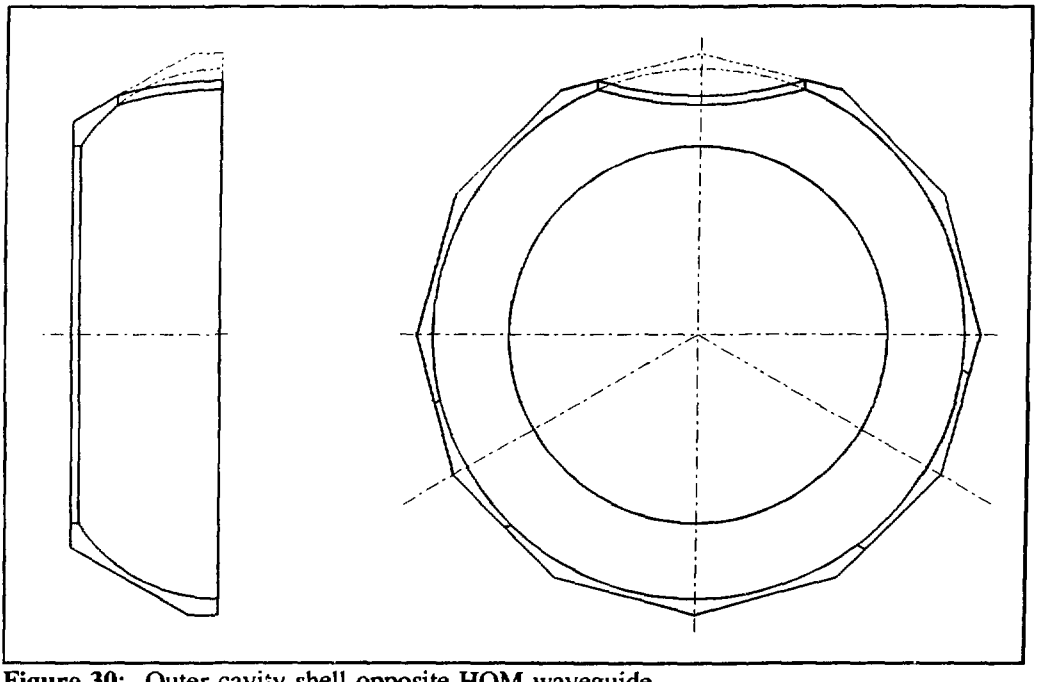

Figure 30: Outer cavity shell opposite HOM waveguide

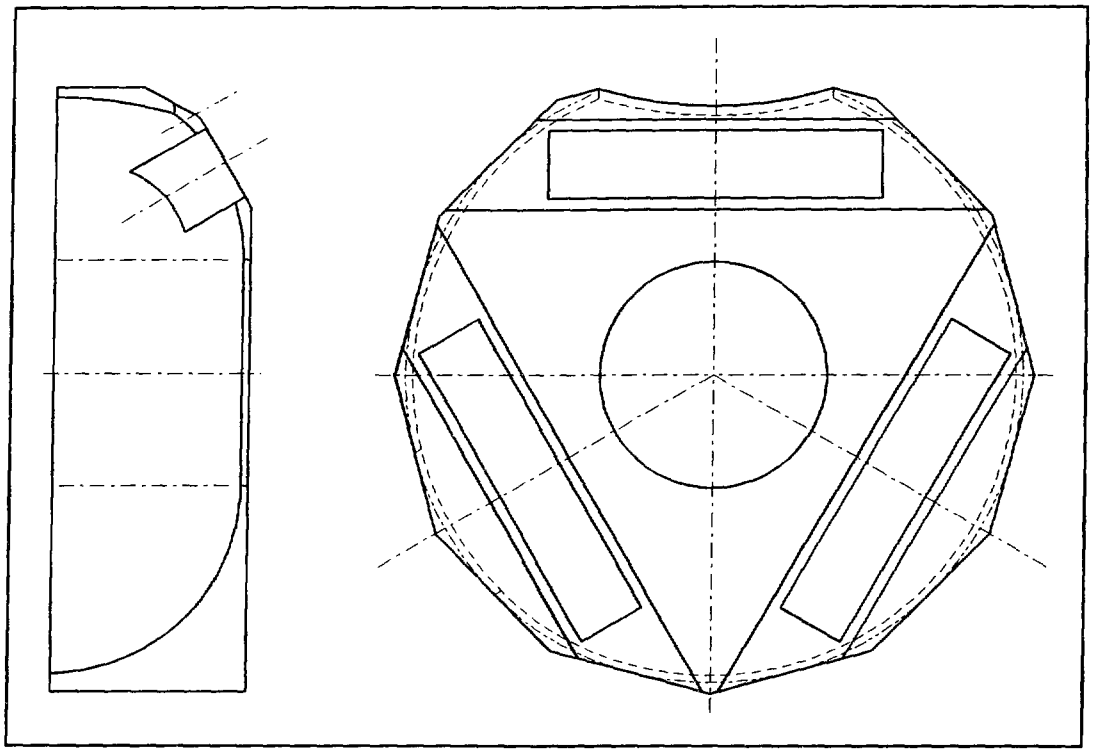

Figure 31: Outer cavity shell on HOM waveguide side

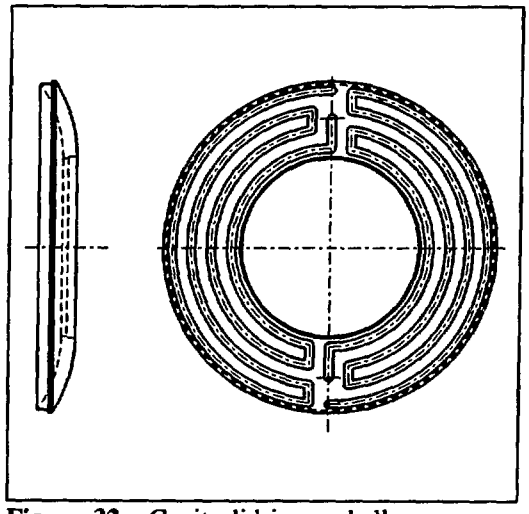

Figure 32: Cavity lid inner shell

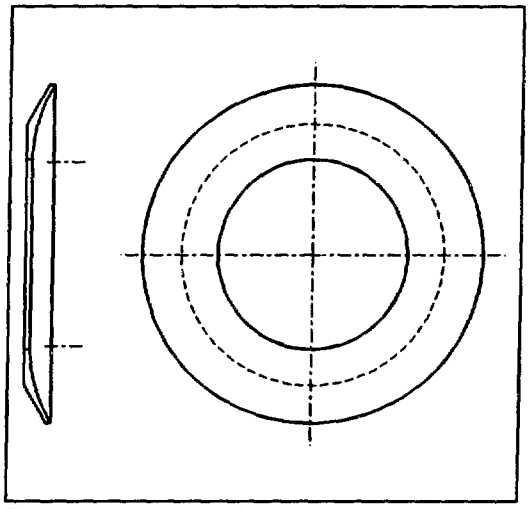

Figure 33: Cavity lid outer shell

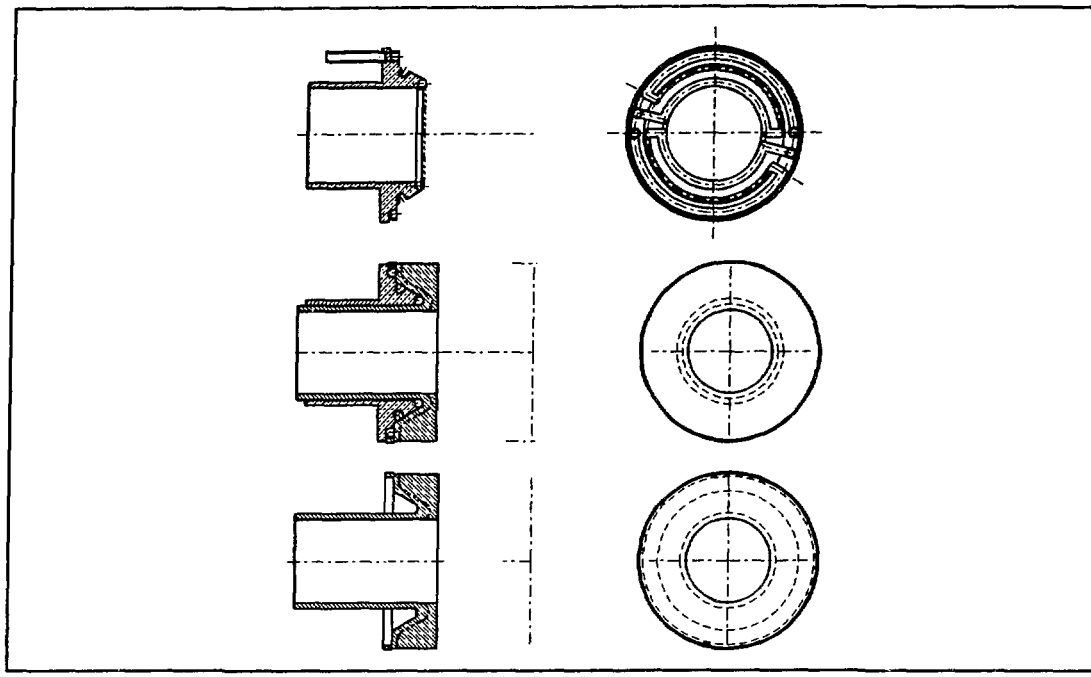

Figure 34: Beam port subassembly, showing details of cooling channels

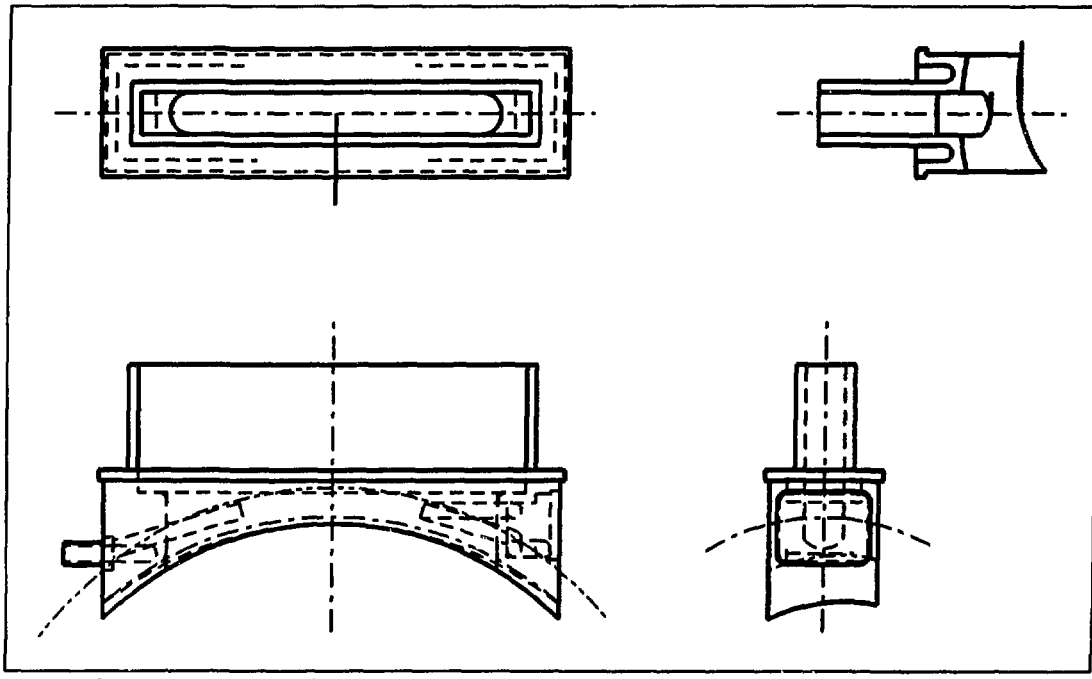

Figure 35: HOM waveguide port subassembly

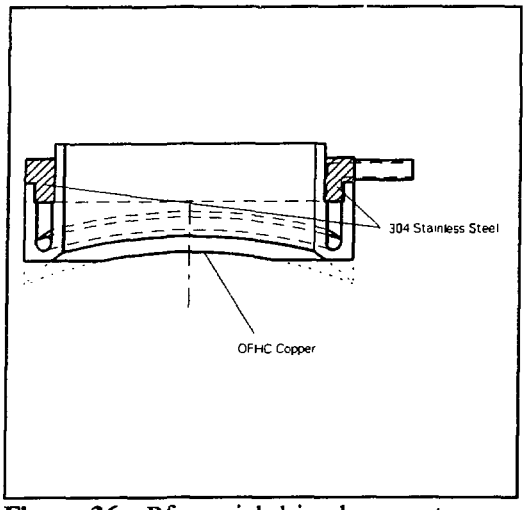

Figure 36: Rf coaxial-drive-loop port

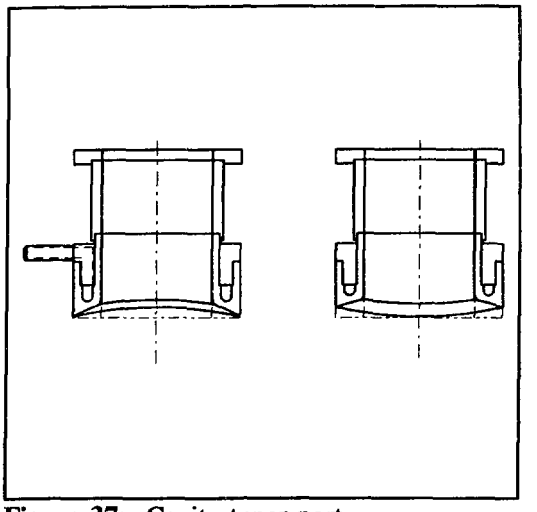

Figure 37: Cavity tuner port

5.2 Materials

5.2.1 OFHC Copper

OFHC Copper is the preferred material for the rf cavity shell. It has excellent electrical and thermal conductivity, and is very suitable for joining with several brazing compounds (allowing for several joining steps and for repairs, if necessary). OFHC copper is already the standard material used on most high-power room-temperature cavities. The main drawbacks with OFHC copper are low yield strength (69 MPa) and poor machinability. With care in design and manufacture, both of these deficiencies can usually be overcome. The low strength does prevent using copper for flanges for attaching other equipment.

5.2.2 Type 304 Stainless Steel

Type 304 stainless steel has good mechanical strength, making it suitable for flanges where

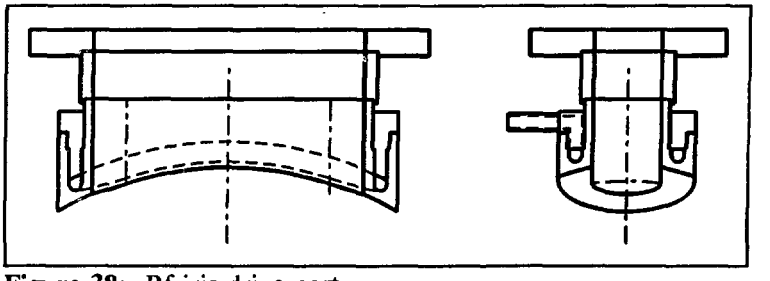

Figure 38: Rf iris-drive port

external fixtures attach to the cavity. This particular stainless steel also has a similar thermal expansion coefficient to that of copper (18.4×10^{-6}/°C compared to 17.6×10^{-6}/°C) [9], so brazing tolerances of less 0.15 mm can be maintained between copper and steel, provided the pieces are not much larger than 200 mm across the joint. Stainless steel must be nickel plated before brazing, to ensure a leak-proof joint. Suitable annealing and machining practices must be used to avoid the possibility of warping during machining of stainless steels.

5.3 Fabrication Methods

5.3.1 Forming

Rough forging followed by machining is the best choice for a prototype cavity. (Some rough forging is necessary before machining, because OFHC copper is not available in thicknesses greater than 12.5 cm.) Precision forging is not an economical option for a prototype cavity, since the cost of producing the required moulds exceeds the cost of machining from a rough forging. However, precision forgings may be economical for the production cavity. Finish machining is still necessary in either case, for dimensional accuracy.

Spinning is an alternative to forging axisymmetric pieces, but the thickness of the blocks before machining may limit its use. Casting is not recommended, because of the unacceptable risk of subsurface porosity. Electroforming, used to fabricate the PEP-II low-power cavity, is probably too slow and expensive to achieve the desired thickness for a high-power cavity.

5.3.2 Joining

Brazing has been used successfully for rf cavities at most accelerator laboratories for many years. Advantages include the ability to join many dissimilar metals (provided there is a close match of thermal expansion coefficients), good mechanical strength, and a smooth joint surface, making this method appropriate for rf cavity manufacture. The disadvantages include demand for tight dimensional tolerances and careful surface preparation at mating surfaces. Since the whole cavity must be raised to the brazing temperature, there is an expansion-contraction cycle and annealing at each brazing stage. Temperature control must

be tight, yet it is preferable to bring a copper work-piece to peak temperature quickly to avoid crystallization.

Electron-Beam welding is an effective way to join metals when the heat-affected zone must be small. Thick sections can be welded, and joint strength is high. However, the part size may be limited because a manipulator must be used in vacuum to position the welding head. It is not clear whether such dissimilar metals as stainless steel and copper can be well joined in this way. If so, the problem of differential thermal expansion goes away. But joint smoothness may be a problem with this technique, creating stress concentrations as sites for fatigue cracking in the coolant channels.

5.4 Cavity Design and Fabrication Plan

This section outlines a mechanical design and fabrication plan for manufacturing a prototype high-power PEP-II cavity. After the method is outlined, some of the more significant details of the design are discussed.

5.4.1 Manufacturing Method

The manufacturing method for the prototype cavity is to:

1) forge copper blanks thick enough to have adequate rigidity and dimensional stability for handling and brazing operations;

main cavity cooling jackets:

2) bore a reference surface flat into the inside of the inner shell blank, as a temporary mounting surface for machining and handling;
3) install helicoils for lifting lugs in the reference flat;
4) rough-turn the inner cooling jacket surface;
5) mill the cooling channels into the inner shell;
6) finish-turn the inner cooling jacket surface;
7) de-burr the edges of the cooling channels;

8) turn a reference surface flat on the outside of the outer shell blank as a temporary mounting surface for machining and handling;
9) install helicoils for lifting lugs in the reference flat;
10) match-machine the outer cooling jacket surface to the inner jacket surface;
11) braze the cooling jacket sandwich of the cavity shell;
12) leak test the cooling channels of the cavity shell;

cavity lid:

13) rough-turn the inner cooling jacket surface;
14) mill the cooling channels into the inner shell of the lid;
15) finish-turn the inner cooling jacket surface;
16) de-burr the edges of the cooling channels;
17) match-machine the outer cooling jacket surface to the inner jacket surface;
18) braze the cooling jacket sandwich of the lid shell;
19) leak-test the cooling channels of the lid shell;
20) rough-turn the inner lid surface;
21) turn the mating surface for the lid/cavity joint;

main cavity inner surface:

22) bore the mating surface for the cavity/lid joint;
23) rough-bore the inner cavity surface using the mating surface for the lid as a set-up reference;

main cavity outer surface:

24) mill the outer surface flats for ports and waveguide;
25) make coolant-tube connectors;
26) mill excess material from cavity shell;
27) machine holes for coolant-tube connectors;
28) machine parts for waveguide and ports (inner surfaces rough machined only);
29) braze waveguide and port subassemblies (with coolant-tube connectors);
30) leak-test waveguide and port subassemblies;

31) mill mating surface for waveguide/cavity joint;
32) mill mating slots for waveguide in cavity;
33) bore holes for ports;
34) braze beam port to lid (unless lid subassembly includes beam port);
35) clamp waveguide and ports (but not lid) to main cavity, with coolant connectors, to temporary support stand;
36) braze waveguide, ports, and coolant connectors to main cavity;

final assembly and testing:

37) assemble and clamp main cavity and lid on temporary stand for tuning;
38) tune clamped assembly, removing the lid for final skimming of the inner surface;
39) braze the cavity assembly;
40) fabricate support stand;
41) mount cavity on support stand;
42) set up test infrastructure;
43) perform vacuum leak-test;
44) perform pressure test;
45) perform pressure-drop-during flow test.

5.4.2 Assembly

Particular areas of concern in manufacture are design of brazed joints, attachment of waveguide and ports, cavity assembly while allowing for tuning, and support stand connections to the cavity.

5.4.2.1 Brazing

All braze joints are designed to adhere to the engineering design criterion that no brazed joint has a path between contact with cooling water and with vacuum. Simple joint geometries are used to ensure tight dimensional tolerances.

5.4.2.2 Attachment of Waveguide and Ports

Assembly of the waveguide presents the greatest challenge in the design of the mating pieces of the cavity. There must be a simple geometry at mating joints to ensure close dimensional tolerances for brazing. Cooling channels are cut into the inner shell from the outside.

The easiest solution is a flat area against which to mate the flange of the waveguide base with the rounded edge of the aperture as part of the inner shell of the cavity. The flat is perpendicular to the long axis of the waveguide. The insert with a "racetrack" iris slot for the waveguide is a separate piece. Cooling channels can be included in two ways: integral with the main cavity, or separate.

Integrated cooling channels can be machined into the mating surface of the insert to meet those of the cavity inner shell, where the thickness of the inner shell is reduced by milling the flat surface. A slot is machined out of the outer shell for the waveguide inner surface to join to the inner cavity shell. A gap must be included to separate the water joint from the vacuum joint. This gap can be monitored to detect leaks.

The recommended design, however, uses waveguide inserts that are separately cooled subassemblies brazed into the cavity. This design avoids having the iris machined into the inner rf shell of the main cavity.

There are three reasons for not making the waveguide corners part of the main cavity: difficulty in machining the waveguide corners inside the bowl of the cavity because of restricted access by a milling head, better quality control (there would be extreme difficulty in repairing poor quality machining, as opposed to making a replacement insert), and difficulty in assembling outside waveguide covers along the direction of beam path. (It is much easier to assemble inserts along the axis of waveguide.) To obviate the problem of a water-vacuum joint, a gap groove is machined along the joint, which can be helium-monitored for leaks. An alternative to a closed gap is a groove with openings to atmosphere spaced around the perimeter.

For the drive-loop coupling and tuning port, being axisymmetric, turning and boring operations are sufficient to produce appropriate shapes and mating surfaces, except for

milling of cooling channels. In these ports, cooling channels are milled into the outside of the inner sleeve, which is more convenient than inserting a tool into a hollow cylinder. The design philosophy is otherwise the same as for a waveguide subassembly insert with separate cooling.

5.4.2.3 Cavity Assembly

There are two alternatives: install ports and waveguide before machining the inner cavity surface, or machine first and then put in waveguide and ports. The recommended approach is to rough-bore the shape of the inner rf shell, attach waveguide and ports (but not the lid on one end), and then finish-bore the rf shell.

The advantages of the first alternative are that appendages can be attached rigidly to the inside of the cavity block for brazing, and joints will be well blended because the final surface of the rf shell is established in a single cutting operation. The disadvantage is that the machining of the inner surface must accommodate the presence of waveguide and ports, necessitating a support jig. More importantly, elastic deflections of the cavity during clamping and machining may result in a deformed inner surface.

The major advantage of the second alternative is having a stiff structure for cutting the inner surface profile. Because it is more important to have an accurate surface profile on the inside of the cavity than on the outside, it is preferable to cut the inner surface first. Elastic deformations on the outer surface during its machining are more acceptable; clamping deformations are of more concern.

The recommended procedure preserves the advantages of both alternatives. A numerical boring machine is used to machine the inner cavity profile. The cylindrical surface of the beam port and lid joints can be used as a reference for the next set-up, machining the holes for ports and waveguide.

A potential disadvantage is joining the ports and waveguide to a relatively thin shell. But substantial mating surfaces should permit local clamping and ensure good alignment. The important disadvantage of this method is the need to machine the ancillary pieces to close tolerances so that the edges of joints line up well on the inner surface. The brazed joint

contributes to the blending of surfaces between joints, but only across the joint itself. A discontinuous step adversely affects the current distribution.

There is a final, rf, tuning step before final brazing. At this time, any deficiencies or corrections in the inner surface geometry to achieve the correct rf operating frequency can be made. It is preferable that tuning be done after the brazing of ports and waveguide. Some support jig is thus necessary to protect the waveguide and port subassemblies. If possible, this tuning should be done with the cavity still affixed to its support jig, making the set-up for final machining easier if required. The fewer set-ups done, the better: less handling of the work-piece reduces the chance of damage, and fewer dimensional errors result from a minimum number of changes of reference points for measurement.

The final structural braze joins the main cavity body to the two end pieces.

In assembly alternatives, removing excess material from the outside of the cavity can be done after brazing the waveguide but before tuning, provided that appendages are not so long that they interfere with the cutter. The dimensional accuracy of outside machined flats is less important than the inner cavity geometry, so some elastic deflections during machining would be acceptable. This material removal should be done before attaching cooling water connections and tubes.

5.5 Cooling Channel Geometry

Finite-element analysis reveals that the water temperature at the radius of the waveguide should be warmer between the waveguide inserts than inside the inserts themselves, and coolest at the insert ends. The cooling channel geometry is routed to give this temperature distribution. Each of the three sections of the cavity has separate sets of cooling channels. The areas of highest heat flux, namely the cavity nose and waveguide irises, have separate cooling channels. This feature reduces the variations in temperature distribution, thereby reducing the peak stresses. In areas of lower heat flux, cooling channels can have wider spacing. The cooling water velocity can be reduced to 3.7 m/s throughout most of the cavity, with 5 m/s velocity around the waveguide inserts and ports where maximum heat transfer is necessary. This increase in water velocity is achieved by decreasing the hydraulic

diameter of the cooling channels in the inserts and ports, keeping the Reynolds number of the coolant approximately constant.

6. SUMMARY

A detailed, 3-dimensional, finite-element, thermal-stress analysis of a proposed design for the PEP-II 476 MHz cavity shows that the maximum computed stress is substantially below (by almost a factor of 2) standard engineering design limits. The maximum stress varies from less than 10 MPa, with just water pressure and vacuum loading, to approximately 50 MPa when thermal effects of 150 kW rf dissipation in the walls are included.

The entire cavity can be fabricated from annealed OFHC copper forgings using standard brazing techniques, with 304 stainless steel used around the outside of all waveguides and ports for additional mechanical strength. The proposed cavity design has ports for a standard, PEP coaxial drive loop and tuning plunger. In addition, provision is made for an iris for using an aperture-coupled rf drive.

Before a detailed design is complete, a final stress analysis should be performed to have a reference calculation for comparison with measurements on the prototype cavity. This calculation should include as much detail of the final design as possible. At a minimum, the effects of the cooling channel geometry, water temperature variations, the coaxial-drive port, and HOM waveguides on only one side of the cavity should be included.

ACKNOWLEDGEMENTS

The authors would like to thank members of the PEP-II group at the Stanford Linear Accelerator Center, Lawrence Berkeley Laboratory and Lawrence Livermore National Laboratory for their many useful and encouraging comments and assistance. In particular, R. Pendleton and K. Ko are thanked for their 3-D rf computations essential for this work, K. Skarpaas and J. Hodgson for their suggestions on the mechanical design and analysis, M. Gerhard for his help in extracting power flux data from the ARGUS code, and M. Zisman, G. Lambertson, R. Rimmer, H. Schwarz and J. Dorfan for keeping the entire team working together with such good spirit.

At Chalk River Laboratories, the authors would like to thank D. Proulx for his assistance in turning pencil sketches into CAD drawings, and S. Baset for his advice and assistance in using the MENTAT and MARC codes and graphics.

REFERENCES

[1] H. Halbach and R.F. Holsinger, "SUPERFISH - A Computer Program for Evaluation of RF Cavities with Cylindrical Symmetry," *Particle Accelerators* 7 (4), 213-222 (1976).

[2] R. Klatt, et al., "MAFIA - A Three Dimensional Electromagnetic CAD System for Magnets, RF Structures, and Transient Wake-Field Calculations," in "1986 Linear Accelerator Conference Proceedings," Stanford Linear Accelerator Center Report 303 (1986 September) pp. 276-278.

[3] A. Mandofsky, "Three-Dimensional Particle Codes and Applications to Accelerators," in *AIP Conference Proceedings 177: Linear Accelerator and Beam Optics Codes, La Jolla Institute 1988*, Charles R. Eminhizer, Ed. (American Institute of Physics, New York, 1988), pp. 137-160.

[4] *An Asymmetric B-Factory Based on PEP*, Stanford Linear Accelerator Center Report 372 (1991 February).

[5] MARC Analysis Research Corporation, Palo Alto, California.

[6] ASME Boiler and Pressure Vessel Code, Section VIII, Division 2 (1977).

[7] S.H. Crandall, N.C. Dahl and T.J. Lardner, eds., "An Introduction to the Mechanics of Solids", McGraw-Hill (1972).

[8] Materials Engineering, pg. 98, 1988 December.

[9] "The Brazing Book", Handy and Harmon, 1985.

Cat. No. CC2-10782E
ISBN 0-660-14985-0
ISSN 0067-0367

To identify individual documents in the series we have assigned an AECL- number to each.

Please refer to the AECL- number when requesting additional copies of this document

from

Scientific Document Distribution Office
Atomic Energy of Canada Limited
Chalk River, Ontario, Canada
K0J 1J0

Price: B

No. au cat. CC2-10782E
ISBN 0-660-14985-0
ISSN 0067-0367

Pour identifier les rapports individuels faisant partie de cette série nous avons assigné un numéro AECL- à chacun.

Veuillez faire mention du numéro AECL- si vous demandez d'autres exemplaires de ce rapport

au

Service de Distribution des Documents Officiels
Énergie atomique du Canada limitée
Chalk River, Ontario, Canada
K0J 1J0

Prix: B

0499-93